Mathematical modelling of microneedle-mediated transdermal delivery of drug nanocarriers into skin tissue and circulatory system

Ben Newell, Wenbo Zhan [*]

School of Engineering, King's College, University of Aberdeen, Aberdeen AB24 3UE, United Kingdom

ARTICLE INFO

ABSTRACT

Microneedle-mediated transdermal delivery using nanocarriers can successfully overcome the barrier of the stratum corneum and protect drugs from elimination in skin tissues. However, the effectiveness of drug delivery to different layers of skin tissues and the circulatory system varies considerably, subject to the properties of the drug delivery system and delivery regime. How to maximise delivery outcomes remains unclear. In this study, mathematical modelling is employed to investigate this transdermal delivery under various conditions, using the skin model that is reconstructed based on the realistic skin anatomical structure. Treatment efficacy is evaluated in terms of drug exposure over time. The modelling results demonstrate the complex dependence of drug accumulation and distribution on the nanocarrier properties, microneedle properties and environment in different skin layers and blood. Specifically, delivery outcomes in the entire skin and blood can be improved by increasing the loading dose and reducing microneedle spacing. However, several parameters need to be optimised with respect to the specific location of the target site in the tissue for better treatment; these include the drug release rate, nanocarrier diffusivity in microneedle and skin tissue, nanocarrier transvascular permeability, nanocarrier partition coefficient between tissue and microneedle, microneedle length, wind speed and relative humidity. The delivery is less sensitive to the diffusivity and physical degradation rate of free drugs in microneedle, and their partition coefficient between tissue and microneedle. Results obtained from this study can be used to improve the design of the microneedle-nanocarrier combined drug delivery system and delivery regime.

1. Introduction

Transdermal drug delivery has been widely applied in clinical practice, such as in the treatment of pain [1], hypertension [2], and Parkinson's disease [3]. Drugs delivered through routine methods are firstly applied on the surface of intact skin and then transported through the stratum corneum (SC) to viable skin tissues, including viable epidermis (VE), papillary dermis (PD) and reticular dermis (RD) in sequence. The microvascular network embedded in the papillary dermis allows drugs to pass through the vessel walls into the circulatory system, and thus reach other tissues and organs of the body. This delivery mode is favoured due to its painless nature [4]. However, the treatment effectiveness could be extremely disappointing, particularly for sending large molecule drugs to deep skin tissues. This is largely due to the stratum corneum, the top surface of the skin which can effectively prevent external substances, such as drugs from entering the body [5].

Microneedles are a promising drug delivery system (DDS) to overcome this barrier by piecing the stratum corneum to reach viable skin tissues. The loaded drugs can then be released directly in a controlled manner to produce therapeutic effects. Various types of microneedles have been developed to suit different applications and delivery conditions [6]. Despite these advances, the treatment remains limited by fast drug elimination due to metabolic reactions, *etc.* With drugs encapsulated inside, nanocarriers have the potential to further prevent the payload from undesired reactions and thereby provide a sustainable drug supply [7]. The feasibility of combining microneedles with nanocarriers has been demonstrated in preclinical trials [8]. However, the delivery outcomes of this combined DDS vary considerably due to the influences of multiple factors, including the properties of microneedles and nanocarriers, and the environment. How to optimise this DDS and delivery regime is yet fully understood.

Drug delivery involves multiple physiological and physicochemical processes that are cross-linked. It would be infeasible or not economically viable to examine each process through *in vivo* experiments. Mathematical modelling provides an alternative solution. Using a set of validated governing equations to describe the drug delivery processes,

---

* Corresponding author.
 E-mail address: w.zhan@abdn.ac.uk (W. Zhan).
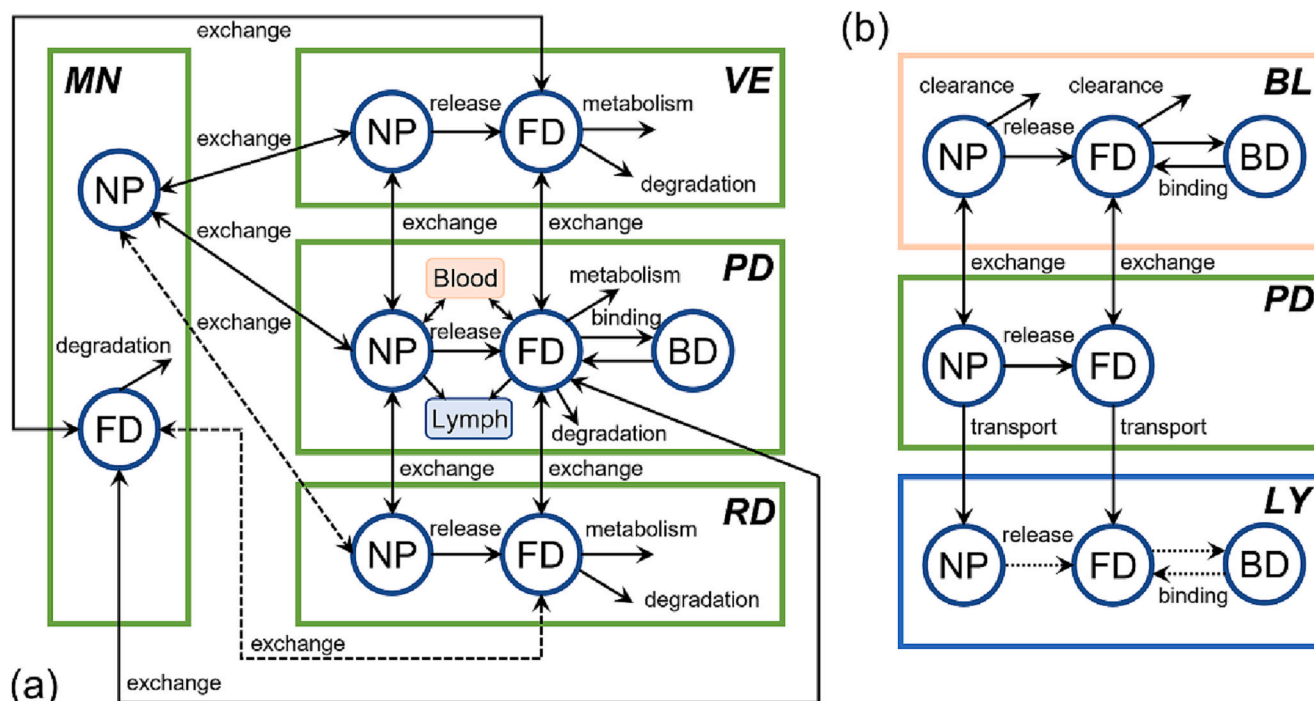
Fig. 1. Drug transport in microneedle-medicated delivery using nanocarriers. The overview of drug transport processes from the microneedle to different layers of skin tissues is shown in (a), with a closer look at the drug transport between the papillary dermis, blood and lymph given in (b). The lymphatic system is treated as a sink for nanocarriers and released drugs. Therefore, the dynamics of drug release and binding with proteins in the lymphatic system are not specified, marked by the dotted line. The drug exchange between the reticular dermis and microneedle depends on the insertion depth and length of the microneedle, marked by the dashed line. Since the proteins involved in the binding process, such as albumin, are mainly from the blood, this process is considered in the papillary dermis. Drug reactions with other proteins are described by metabolic reactions in an integrated manner. This diagram only presents the transport processes, not referring to the realistic dimension of the skin layers.

this research method allows studying the effect of each influencing factor individually and in an integrated manner [9,10]. Comprehensive parametric studies can also be carried out to compare the delivery outcomes under different conditions to identify the optimum. Mathematical models have been established on different scales to study drug transport and accumulation in the skin. Assuming each skin layer as a homogeneous compartment [11], kinetic models can effectively describe drug exchange between linked compartments for fast predicting the time courses of drug concentration; however, spatial distributions of drugs in skin layers are unavailable. Models on the microscale are developed to focus on drug transport and deposition in tissue microstructure over time and location [12,13]. They are consequently hard to reflect delivery outcomes in multiple skin layers since the computational domain is usually a few micrometres large. This limitation can be overcome with tissue-scale models, where the skin layers are treated as separate media of drug transport, accommodating the anatomy of the skin. In the study by Calcutt et al., a tissue-scale model was employed to reveal the function of the superficial subpapillary dermal plexus while considering drug transport in the upstream layer of the viable dermis and the downstream layer of the reticular dermis [14]. Anissimov et al. identified the importance of blood and lymphatic transport in drug dermal diffusion by examining the delivery of six different drugs to the skin [15]. Machekposhti et al. simulated microneedle-mediated transdermal delivery of plain drugs and found good agreement between the modelling and experiment results [16].

In this study, a tissue-scale model is applied to simulate the microneedle-mediated transdermal delivery using nanocarriers. The mathematical model incorporates the key delivery processes, including the interstitial fluid flow in skin tissue, water loss to the atmosphere, transport of nanocarriers and released free drugs in microneedles and tissues by diffusion and/or convection, drug release dynamics, drug metabolic reactions and physical degradation, fluid and drug exchange

between skin tissues, blood and lymph, and drug binding with proteins. The delivery outcomes are evaluated in terms of drug exposure over time using the predicted drug concentration. A general microneedle and nanocarrier are used without specifying the type and formulation. This enables performing exploratory parametric studies to examine the impact of a range of different properties of microneedles and nanocarriers.

2. Materials and method

2.1. Mathematical model

The modelling framework consists of the governing equations for the transport of interstitial fluid and drugs in different forms in and between the microneedles, skin tissues and circulatory systems. Stratum corneum is a lipid-protein biphasic structure made up of layers of corneocytes that are sealed by densely packed lipids, making it nearly impermeable to most substances including small molecule drugs [17]. Although water molecules can pass through the stratum corneum, the transport mechanisms differ from that in the viable skin tissue [18]. Therefore, this study is mainly focused on viable skin tissues, while the water flux through the stratum corneum is considered in terms of trans-epidermal water loss. The details of the mathematical model are given below.

2.1.1. Transport model of interstitial fluid

The viable skin tissues are considered porous media, where the incompressible, Newtonian interstitial fluid flow can be described by the continuity equation and momentum equation, as

$$\nabla \bullet \mathbf{v}_{is} = \begin{cases} F_{bl} - F_{ly}, & \text{in PD} \\ 0, & \text{in VE and RD} \end{cases} \tag{1}$$

$$\rho_{is}\left(\frac{\partial \mathbf{v}_{is}}{\partial t}+\mathbf{v}_{is}\bullet\nabla\mathbf{v}_{is}\right)=-\nabla p_{is}+\mu_{is}\nabla^2\mathbf{v}_{is}-\frac{\kappa_{tis}}{\mu_{is}}\mathbf{v}_{is} \qquad (2)$$

where ρ_{is} and μ_{is} are the density and viscosity of the interstitial fluid, respectively. p_{is} is the pressure and $\mathbf{v}_{is}$ is the flow velocity. κ_{tis} is the tissue permeability. Two horizontal plexuses are present in the papillary dermis and deep reticular dermis, respectively. Since drug transport into the circulating systems mainly occurs through the papillary plexus which is closer to the administration site, the latter one located in the deep tissue is not considered [14]. The fluid loss from the blood (F_{bl}) is governed by Starling's law [19], as

$$F_{bl}=L_{bl}\frac{S_{bl}}{V_{tis}}\left[p_{bl}-p_{is}-\sigma_T(\pi_{bl}-\pi_{is})\right] \qquad (3)$$

where L_{bl} is the hydraulic conductivity of the microvasculature wall. S_{bl}/V_{tis} stands for the microvasculature density, defined as the surface area of the microvasculature wall per tissue volume. p_{bl} is the pressure of blood. σ_T is the osmotic reflection coefficient due to the proteins in the blood. π_{bl} and π_{is} are the osmotic pressure of the blood and interstitial fluid, respectively. Since lymphatic vessels run parallel to the blood vessels in the papillary dermis [20], the fluid loss to the lymphatic system in this skin layer can be calculated [21] by

$$F_{ly}=L_{ly}\frac{S_{ly}}{V_{tis}}\left(p_{is}-p_{ly}\right) \qquad (4)$$

where L_{ly} is the hydraulic conductivity of the lymphatic vessel wall, and S_{ly}/V_{tis} is the surface area of the lymphatic vessel wall in unit tissue volume. p_{ly} is the lymphatic pressure.

2.1.2. Transport model of drugs

The transport of therapeutic agents in the microneedle (MN), skin layers, blood (BL) and lymph (LY) is schematically illustrated in Fig. 1. The letters NP, FD and BD refer to nanocarrier-encapsulated drugs, free drugs and drugs that are bound with proteins, respectively.

2.1.2.1. Drug transport in microneedle.
Nanocarriers are assumed to be stable before entering the skin tissue. Therefore, the nanocarrier concentration in MN ($C_{NP,MN}$) is determined by the diffusive transport, as

$$\frac{\partial C_{NP,MN}}{\partial t}=D_{NP,MN}\nabla^2 C_{NP,MN} \qquad (5)$$

where $D_{NP,MN}$ is the nanocarrier diffusivity in the microneedle. Similarly, the concentration of free drugs in the microneedle ($C_{FD,MN}$) is subject to its diffusivity ($D_{FD,MN}$) and physical degradation rate ($k_{d,MN}$), as

$$\frac{\partial C_{FD,MN}}{\partial t}=D_{FD,MN}\nabla^2 C_{FD,MN}-k_{d,MN}C_{FD,MN} \qquad (6)$$

2.1.2.2. Drug transport in viable epidermis.
Nanocarriers transfer in the viable epidermis by convection with the interstitial fluid flow, diffusion driven by the concentration gradient, and drug release. The concentration ($C_{NP,VE}$) can be calculated by

$$\frac{\partial C_{NP,VE}}{\partial t}=D_{NP,VE}\nabla^2 C_{NP,VE}-\nabla\bullet\left(\mathbf{v}_{is}C_{NP,VE}\right)-k_{rel,VE}C_{NP,VE} \qquad (7)$$

where $D_{NP,VE}$ is the nanocarrier diffusivity in the viable epidermis, and $k_{rel,VE}$ is the local drug release rate. The concentration of free drugs ($C_{FD,VE}$) in this layer is determined by diffusion and convection, drug release, metabolic reactions and physical degradation, as

$$\frac{\partial C_{FD,VE}}{\partial t}=D_{FD,VE}\nabla^2 C_{FD,VE}-\nabla$$
$$\bullet\left(\mathbf{v}_{is}C_{FD,VE}\right)+k_{rel,VE}C_{NP,VE}-\frac{V_{max}C_{FD,VE}}{v_m+C_{FD,VE}}-k_{d,VE}C_{FD,VE} \qquad (8)$$

where $D_{FD,VE}$ is the free drug diffusivity in the viable epidermis. V_{max} and v_m are the constant rates of metabolic reactions. $k_{d,VE}$ is the local physical degradation rate.

2.1.2.3. Drug transport in papillary dermis.
The transport of nanocarriers in the papillary dermis depends on the diffusive and convective transport in the tissue interstitium, drug exchange with the blood, loss to the lymph, and drug release. The concentration ($C_{NP,PD}$) can be calculated by

$$\frac{\partial C_{NP,PD}}{\partial t}=D_{NP,PD}\nabla^2 C_{NP,PD}-\nabla$$
$$\bullet\left(\mathbf{v}_{is}C_{NP,PD}\right)-k_{rel,PD}C_{NP,PD}-Ex\left(C_{NP,BL},C_{NP,PD}\right)-F_{ly}C_{NP,PD} \qquad (9)$$

where $D_{NP,PD}$ stands for the diffusivity of nanocarriers in the papillary dermis. $k_{rel,PD}$ is the local drug release rate. $Ex\left(C_{NP,BL},C_{NP,PD}\right)$ is the exchange rate of nanocarriers between the skin tissue and blood, defined as

$$Ex\left(C_{NP,BL},C_{NP,PD}\right)=P_{NP}\frac{S_{bl}}{V_{tis}}\left(C_{NP,PD}-C_{NP,BL}\right)\frac{Pe_{tb,NP}}{e^{Pe_{tb,NP}}-1}-F_{bl}(1-\sigma_{NP})C_{NP,BL} \qquad (10)$$

in which P_{NP} is the transvascular permeability of nanocarriers. σ_{NP} is its reflection coefficient. $C_{NP,BL}$ is the nanocarrier concentration in the blood. $Pe_{tb,NP}$ is the Péclet number, defined as

$$Pe_{tb,NP}=\frac{F_{bl}(1-\sigma_{NP})}{P_{NP}S_{bl}/V_{tis}} \qquad (11)$$

The concentration of free drugs ($C_{FD,PD}$) in this skin layer is determined by the diffusive and convective transport in the tissue interstitium, release from nanocarriers, metabolic reactions and physical degradation, binding with the proteins that are transported by the blood (*e.g.* albumin), drug exchange between the skin tissue and blood, and loss to the lymph, as

$$\frac{\partial C_{FD,PD}}{\partial t}=D_{FD,PD}\nabla^2 C_{FD,PD}-\nabla\bullet\left(\mathbf{v}_{is}C_{FD,PD}\right)+k_{rel,PD}C_{NP,PD}$$
$$-\frac{V_{max}C_{FD,PD}}{v_m+C_{FD,PD}}-k_{AR}C_{FD,PD}+k_{DR}C_{BD,PD}-Ex\left(C_{FD,BL},C_{FD,PD}\right)$$
$$-F_{ly}C_{FD,PD}-k_{d,PD}C_{FD,PD} \qquad (12)$$

where $D_{FD,PD}$ is the diffusivity of free drugs in the papillary dermis. k_{AR} and k_{DR} are the association and disassociation rate of drugs with the proteins, respectively. $k_{d,PD}$ is the local physical degradation rate. The exchange rate of $Ex\left(C_{FD,BL},C_{FD,PD}\right)$ has the same definition in Eq. (10) using the concentration and properties of free drugs. $C_{FD,BL}$ is the free drug concentration in the blood. The concentration of bound drugs ($C_{BD,PD}$) is governed by

$$\frac{dC_{BD,PD}}{dt}=k_{AR}C_{FD,PD}-k_{DR}C_{BD,PD} \qquad (13)$$

2.1.2.4. Drug transport in reticular dermis.
Nanocarriers transport in the reticular dermis by diffusion and convection with the interstitial fluid flow. Its concentration ($C_{NP,RD}$) is also subject to local drug release,

$$\frac{\partial C_{NP,RD}}{\partial t}=D_{NP,RD}\nabla^2 C_{NP,RD}-\nabla\bullet\left(\mathbf{v}_{is}C_{NP,RD}\right)-k_{rel,RD}C_{NP,RD} \qquad (14)$$

where $D_{NP,RD}$ is the local diffusivity of nanocarriers. $k_{rel,RD}$ is the drug release rate from nanocarriers in the reticular dermis. The concentration of free drugs in the reticular dermis is determined by diffusion and convection, drug release, metabolic reactions and physical degradation, as
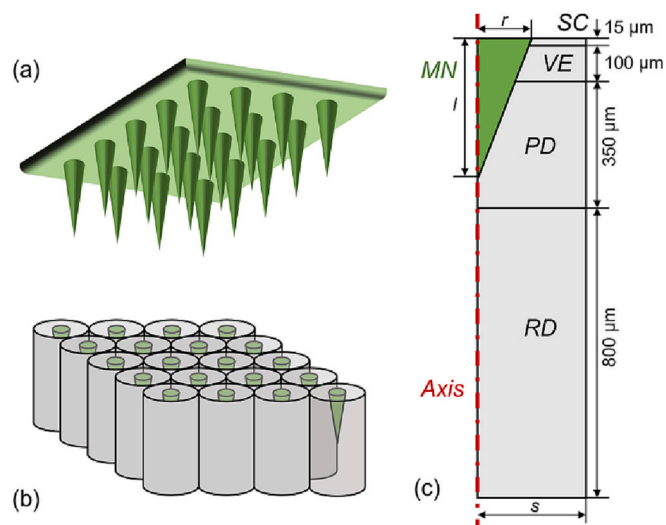
Fig. 2. Model geometry. (a) Microneedle array on the supporting patch, (b) schematic diagram of the aggregation of representative elementary volume (REVs), and (c) computational domain for simulation. The microneedle and skin tissue are marked in dark green and grey, respectively. r and l are the radius and length of the microneedles. Given microneedles are evenly distributed in the patch with the same distance between each other, a REV can be applied to represent the delivery outcome. The REV is axially symmetric with a radius, s, equal to half the distance between two adjacent microneedles. (For interpretation of the references to colour in this figure legend, the reader is referred to the web version of this article.)

$$\frac{\partial C_{FD,RD}}{\partial t} = D_{FD,RD}\nabla^2 C_{FD,RD} - \nabla$$

$$\bullet \left(\mathbf{v}_{is}C_{FD,RD}\right) + k_{rel,RD}C_{NP,RD} - \frac{V_{max}C_{FD,RD}}{v_m + C_{FD,RD}} - k_{d,RD}C_{FD,RD} \quad (15)$$

where $D_{FD,RD}$ is the diffusivity of free drugs in the reticular dermis. $k_{d,RD}$ is the local physical degradation rate.

2.1.2.5. Drug transport in blood. After entering the blood, nanocarriers can also continuously release the payload and be cleared by the organs such as the kidney. The concentration ($C_{NP,BL}$) can be calculated by

$$\frac{dC_{NP,BL}}{dt} = \frac{V_{PD}N}{V_{dis,NP}}Ex\left(C_{NP,BL}, C_{NP,PD}\right) - k_{rel,BL}C_{NP,BL} - k_{clr,NP}C_{NP,BL} \quad (16)$$

where $k_{rel,BL}$ is the drug release rate in the blood. $k_{clr,NP}$ is the plasma clearance rate. V_{PD} is the volume of the papillary dermis surrounding each microneedle, and $V_{dis,NP}$ is the distribution volume of nanocarriers. N is the number of microneedles in a patch.

The concentration of free drugs in the blood ($C_{FD,BL}$) is determined by the exchange with skin tissue, drug release from nanocarriers, plasma clearance and the two-way interaction with the proteins, as

$$\frac{dC_{FD,BL}}{dt} = \frac{V_{PD}N}{V_{dis,FD}}Ex\left(C_{FD,BL}, C_{FD,PD}\right) + k_{rel,BL}C_{NP,BL} - k_{clr,FD}C_{FD,BL}$$

$$- k_{AR}C_{FD,BL} + k_{DR}C_{BD,BL} \quad (17)$$

in which $V_{dis,FD}$ is the distribution volume of free drugs. $k_{clr,FD}$ is the plasma clearance rate of free drugs. The concentration of bound drugs in the blood ($C_{BD,BL}$) is governed by

$$\frac{dC_{BD,BL}}{dt} = k_{AR}C_{FD,BL} - k_{DR}C_{BD,BL} \quad (18)$$

Table 1
Model parameter for tissue properties.

Symbol	Parameter	Unit	VE	PD	RD	Source
κ_{tis}	Permeability to interstitial fluid	m^2	1.0×10^{-16}	1.0×10^{-16}	1.0×10^{-16}	[25]
μ_{is}	Viscosity of interstitial fluid	Pa·s	7.8×10^{-4}	7.8×10^{-4}	7.8×10^{-4}	[26]
ρ_{is}	Density of interstitial fluid	kg/m^3	1000	1000	1000	[27]
π_{bl}	Osmotic pressure of blood	Pa	–	2670	–	[21]
π_{is}	Osmotic pressure of interstitial fluid	Pa	–	1330	–	[21]
σ_T	Osmotic reflection coefficient for blood proteins	–	–	0.91	–	[21]
L_{bl}	Hydraulic conductivity of the blood vessel wall	m/Pa/s	–	2.7×10^{-12}	–	[21]
p_{bl}	Intracapillary pressure	Pa	–	2080	–	[21]
S_{bl}/V_{tis}	Capillary surface area per tissue volume	m^{-1}	–	6.0×10^3	–	[28]
$L_{ly}S_{ly}/V_{tis}$	Transport rate of interstitial fluid to lymphatics	Pa^{-1} s^{-1}	–	4.2×10^{-7}	–	[21]
p_{ly}	Intra-lymphatic pressure	Pa	–	0	–	[21]

Table 2
Model parameters for therapeutic agent properties.

Symbol	Parameter	Unit	Nanocarrier	Free drug
D_{MN}	Diffusivity in MN	m^2/s	1.0×10^{-13} [29]	1.0×10^{-10} [30]
D_{tis}	Diffusivity in tissue of VE, PD and RD	m^2/s	1.0×10^{-13} [25]	1.0×10^{-10} [25]
K	Partition coefficient between MN and tissue of VE, PD and RD	–	1.0 [9]	1.0 [9]
k_{rel}	Drug release rate from nanocarriers	s^{-1}	1.0×10^{-4} [31]	–
k_d	Drug degradation rate	s^{-1}	–	5.6×10^{-6} [32]
V_{max}	Michaelis–Menten parameter for metabolic reaction	mol /m^3/s	–	0.512 [33]
v_m	Michaelis–Menten parameter for metabolic reaction	mol/m^3	–	6.7×10^{-3} [33]
σ	Osmotic reflection coefficient for blood proteins	–	1.0 [34]	0.15 [26]
k_{AR}	Association rate of drugs with proteins	s^{-1}	–	0.833 [35]
k_{DR}	Dissociation rate of drugs with proteins	s^{-1}	–	0.278 [35]
P	Vascular permeability	m/s	1.0×10^{-9} [36]	3.8×10^{-7} [25]
C_{in}	Administration dose	M	1.0 [37]	–
k_{clr}	Clearance rate in blood	s^{-1}	5.0×10^{-5} [25]	1.0×10^{-4} [25]
V_{dis}	Distribution volume	m^3	1.8×10^{-2} [25]	2.0×10^{-2} [25]

2.2. Model geometry

Since multiple microneedles in the array are usually evenly distributed on the support patch, a representative elementary volume (REV) can be selected, as depicted in Fig. 2. The governing equations of microneedle-mediated transdermal delivery of nanocarrier-encapsulated drugs are solved in this 2D axis-symmetric configuration with the realistic thickness of the stratum corneum (15 μm), viable epidermis (100 μm) and papillary dermis (350 μm) [12,14]. The reticular dermis is 800 μm thick, which is half of the distance between the papillary plexus and reticular plexus [14]. The morphological characteristics of microneedles, including the distance, width and length, can vary considerably depending on the design and fabrication [22,23]. In the baseline study, 10×10 tapered microneedles are spaced 600 μm apart, with a representative radius and length of 150 μm and 390 μm, respectively. These microneedles are long enough to reach the papillary dermis; the impact of morphological properties will be discussed in the following parametric studies. The final computational mesh consists of approximately 41,000 triangular elements, obtained after the mesh independence test. The finest elements with a dimension of 0.006 μm are imposed on the microneedle-tissue interface for generating high-resolution predictions.

2.3. Model parameter

Given the time window of simulated drug delivery processes is much smaller as compared to the tissue growth rate, the properties of tissues and therapeutic agents are treated as constant over time. Baseline values of model parameters together with the sources are summarised in Table 1 and Table 2 for skin tissues and therapeutic agents, respectively. Doxorubicin is selected as a representative drug [24]. The justification for selecting the range and baseline value of some key parameters is provided in the following sections where the impacts of the parameter are examined. The parameterisation of the rest key properties is specified below.

2.3.1. Capillary surface area per tissue volume

Since drug transport from the skin to the circulatory system by crossing the capillary wall, the surface area of the capillaries directly determines the delivery outcomes to the blood and other organs and tissues. However, report of this parameter in human skin is scarce. The average capillary surface area (S_b) of the whole human body was reported to be 100 cm^2/g [28]. Given that the tissue density is 1055 kg/m^3 [38], the average S_b/V is calculated as 10550 m^{-1}. On the other hand, skin capillary surface area was considered half of the skeletal muscle value [39]. Given that the reported capillary surface area of human skeletal muscle was 83.8 cm^2/g [28], the skin S_b/V is estimated to be 4420 m^{-1}. Moreover, heart might be considered as the next best model in the absence of skin data [28]. The capillary surface area of dog and rat's heart were found to be 560 cm^2/g and 600 cm^2/g [28], respectively; their heart S_b/V are 5908 m^{-1} and 6330 m^{-1}. Hence, a representative value of 6000 m^{-1} is used in this study.

2.3.2. Diffusivity of free drugs in tissue

Diffusivity measures the ability of drug particles to transfer in tissues due to thermal motion. Driven by the gradient of drug concentration, this transport property is determined by several factors, including particle size and interstitial fluid viscosity. The diffusivity of small molecule drugs in tissues (m^2/s) can be estimated by [40].

$$D = 1.778 \times 10^{-8}(MW)^{-0.75} \ (32 < MW < 69000) \quad (19)$$

where MW is the drug's molecular weight (g/mol). The calculated diffusivity of the representative drug, doxorubicin is 1.58×10^{-10} m^2/s given its molecular weight is 544 g/mol [41]. This parameter was estimated to be 9.96×10^{-11} m^2/s in Ref. [35]. Therefore, the value of 1.0×10^{-10} m^2/s is adopted.

2.4. Boundary conditions

Water escapes through the stratum corneum passively to the external environment in the form of vapour, known as trans-epidermal water loss (TEWL). The flux (f_{TEWL}) highly depends on the ambient relative humidity (RH) and air velocity (u_{air}) [18], as

$$f_{TEWL} = k_g \frac{(a_w - RH)p_{sat}^o MW}{RT} \quad (20)$$

where $p_{sat}^o = 4.76$ kPa is the water-saturated vapour pressure at the stratum corneum surface. Temperature $T = 305.2$K. Water molecular weight $MW = 18$ g/mol. $R = 8.314$ J/mol/K is the gas constant. The mass transfer rate $k_g = 9.056 \times 10^{-3} D_{air}^{2/3} \sqrt{u_{air}/L}$(m/s) is determined by the water diffusivity in the air $D_{air} = 2.6 \times 10^{-5}$ m^2/s and the characteristic length $L = 1.34 \times 10^{-1}$ m [18]. a_w is the ambient relative humidity at the skin surface, which could be quite close to RH when reaching dynamic equilibrium. The dependence of f_{TEWL} on RH can be expressed by an empirical formula [18], as

$$f_{TEWL} = -2.25 exp\left(\frac{RH}{3.18}\right) - 2.97 \times 10^{-3} exp\left(\frac{RH}{1.34 \times 10^{-1}}\right) - 1.41$$
$$\times 10^{-15} exp\left(\frac{RH}{2.79 \times 10^{-2}}\right) + 1.64 \times 10^1 \ (g/m^2/hr) \quad (21)$$

Following the principle of mass conservation, this TEWL flux of evaporated water at the stratum corneum surface will be in equilibrium with the flux of water flowing from the viable epidermis to the stratum corneum. Therefore, the flux f_{TEWL} is imposed at the interface between the stratum corneum and viable epidermis. Because the stratum corneum is nearly impermeable to most drugs and nanocarriers, the local fluxes of therapeutic agents are assumed to be zero, as

$$-D_{NP,tis}\frac{\partial C_{NP,tis}}{\partial n} = 0; \ -D_{FD,tis}\frac{\partial C_{FD,tis}}{\partial n} = 0 \quad (22)$$

where the subscript tis refers to the local tissue. Drug flux at the top surface of the microneedle is set to be zero due to the assumption that drugs are well contained in the microneedles with no loss to the environment. The transport of nanocarriers and free drugs at the microneedle-tissue interface follows the relationships, as

$$C_{NP,tis} = K_{NP}C_{NP,MN}; \quad -D_{NP,tis}\frac{\partial C_{NP,tis}}{\partial n} = -D_{NP,MN}\frac{\partial C_{NP,MN}}{\partial n}$$
$$C_{FD,tis} = K_{FD}C_{FD,MN}; \quad -D_{FD,tis}\frac{\partial C_{FD,tis}}{\partial n} = -D_{FD,MN}\frac{\partial C_{FD,MN}}{\partial n} \quad (23)$$

where K_{NP} and K_{FD} are the partition coefficient of nanocarriers and free drugs between the skin tissues and microneedles, respectively. The microneedle surface is treated as a wall with no slip for the interstitial fluid flow. Variables at the interfaces between the skin layers are continuous [25,42], whereas the symmetric boundary condition is applied at the side of REV. The boundary condition of zero interstitial fluid flux is specified at the bottom of the domain. This is because, as defined in Fig. 2, the thickness of the reticular dermis is half of the distance between the papillary dermis and the reticular plexus, both of which enable fluid exchange between the blood and tissue. The drug flux at the bottom is also zero since the variation of drug concentration in the deep skin tissue is small [14].

2.5. Numerical methods

The governing equations are implemented in COMSOL Multiphysics (COMSOL Inc., Stockholm, Sweden), a Finite-Element Method-based code package for generating numerical solutions. A fixed time step of
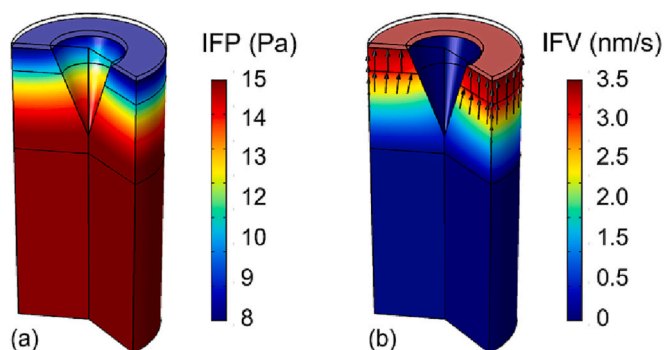
Fig. 3. Interstitial fluid flow in the skin tissues at the baseline condition. (a) Interstitial fluid pressure, IFP and (b) Interstitial fluid velocity, IFV. The vectors of interstitial fluid flow are shown as the arrows in black.

0.001s is applied after conducting the time-step independence test. The fluid transport model is solved in the first place to generate a steady-state solution. The obtained interstitial fluid pressure and velocity are then imported into the drug transport model for simulating the transport and accumulation of nanocarriers and released drugs in and between the microneedles, multiple skin layers and the circulatory systems in a transient manner. All drugs are maintained in the nanocarrier-encapsulated form within the microneedle at the beginning of the treatment. The initial drug concentrations are zero in all the tissue compartments, including different skin layers and blood.

2.6. Quantification of delivery outcomes

The outcomes of transdermal delivery using the microneedle-nanocarrier combined DDS under different conditions are evaluated by the quantitative indexes defined below.

2.6.1. Spatial-averaged concentration

The concentrations of nanocarriers and released free drugs are determined by the cross-linked physiological and physicochemical processes described in Fig. 1, and vary across the skin layers. The spatial-averaged concentration ($\overline{C}$) is applied to reflect the drug accumulation in the compartments including each skin layer, blood and microneedle, as

$$\overline{C} = \frac{\sum C_i V_i}{\sum V_i} = \frac{\sum C_i V_i}{V} \tag{24}$$

where C_i and V_i are the local drug concentration and local volume, respectively. V is the total volume of the studied compartment.

2.6.2. Drug exposure over time

The treatment efficacy can be evaluated by drug exposure over time (*AUC*). It is defined as the area under the curve of the time course of spatial-averaged concentration of free drugs $\overline{C}_{FD}$, as

$$AUC = \int_0^t \overline{C}_{FD}(\tau)d\tau \tag{25}$$

where *t* is the examined duration of treatment.

3. Results

3.1. Baseline study

Nanocarriers and free drugs travel in the tissue interstitium, which is filled with interstitial fluid. Governing equations are solved in the computational domain to obtain the interstitial fluid flow in the skin layers, subject to the tissue properties summarised in Table 1 and the boundary conditions. Fig. 3 shows the flow at baseline conditions of 80% relative humidity and 0.1m/s air velocity [18]. Interstitial fluid pressure (IFP) is uniformly distributed in the reticular dermis and gradually decreases through the papillary dermis and viable epidermis to a minimum on the interface between the stratum corneum and viable epidermis. Interstitial fluid velocity exhibits an opposite pattern. As shown by the vectors, interstitial fluid flows from the deep tissue towards the skin surface. These patterns can be attributed to the distribution of microvasculature in the skin. Since the capillaries mainly exist in the papillary dermis, the fluid exchange between the blood and tissue, and the water loss to the environment take place in the upper skin layers. The interstitial fluid flow in the deep dermis is less influenced.

The spatial distributions of nanocarriers at different time points are represented in Fig. 4 (a). Nanocarriers can successfully enter the tissue interstitium by passing through the microneedle-tissue interface, driven by the concentration difference between the microneedle and surrounding skin tissues. The decrease in concentration in the microneedle occurs first at the tip and gradually spreads to the base as time proceeds. Results show that most nanocarriers can be delivered to the skin in 48 h. Given in Fig. 4 (b) are the spatial distributions of free drugs. Although nanocarriers are stable before entering the skin, the concentration of free drugs is significantly high in the microneedle compared to the skin
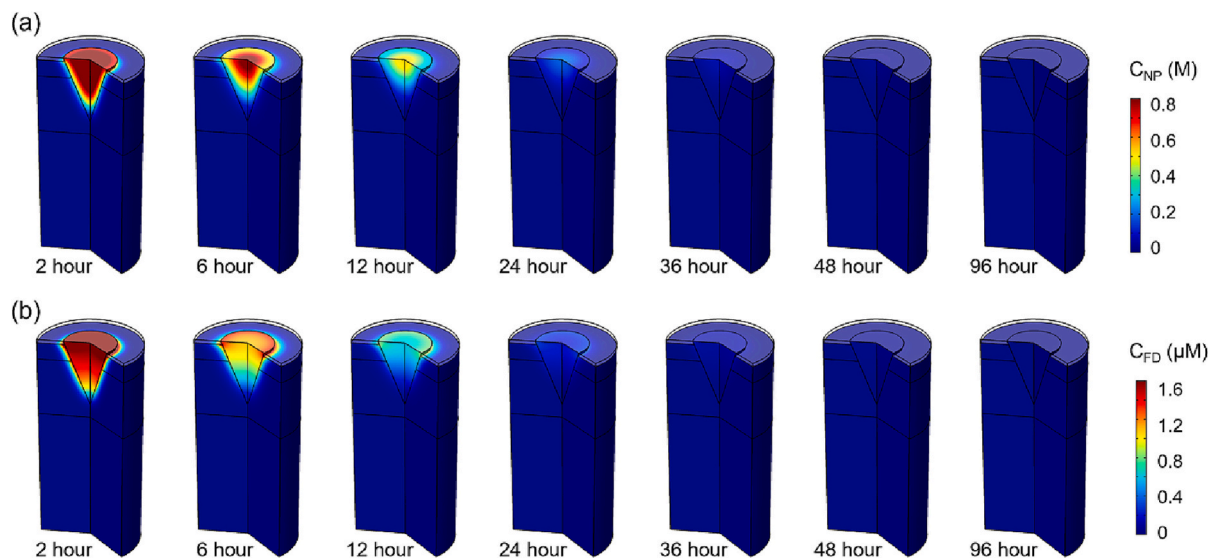
Fig. 4. Spatial distribution of nanocarriers (a) and released free drugs (b) in the microneedle and skin tissues.
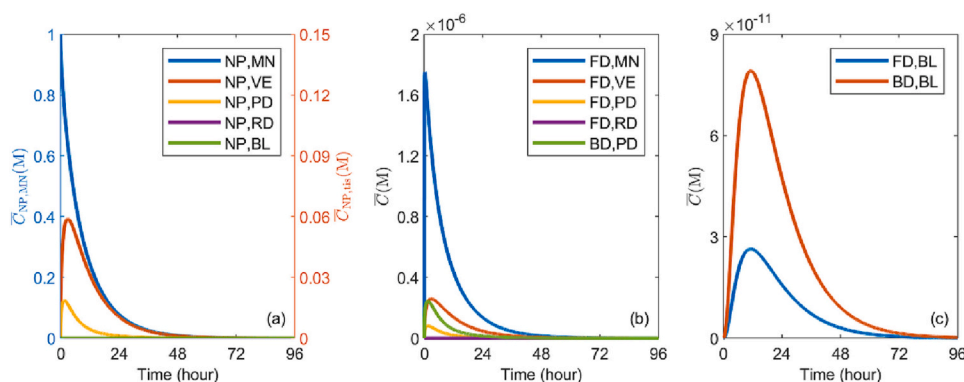
Fig. 5. Time courses of spatial-averaged drug concentrations. (a) Nanocarrier concentration in the microneedle, skin layers and blood. Concentrations of the released drug in (b) microneedle and skin tissues and (c) blood.
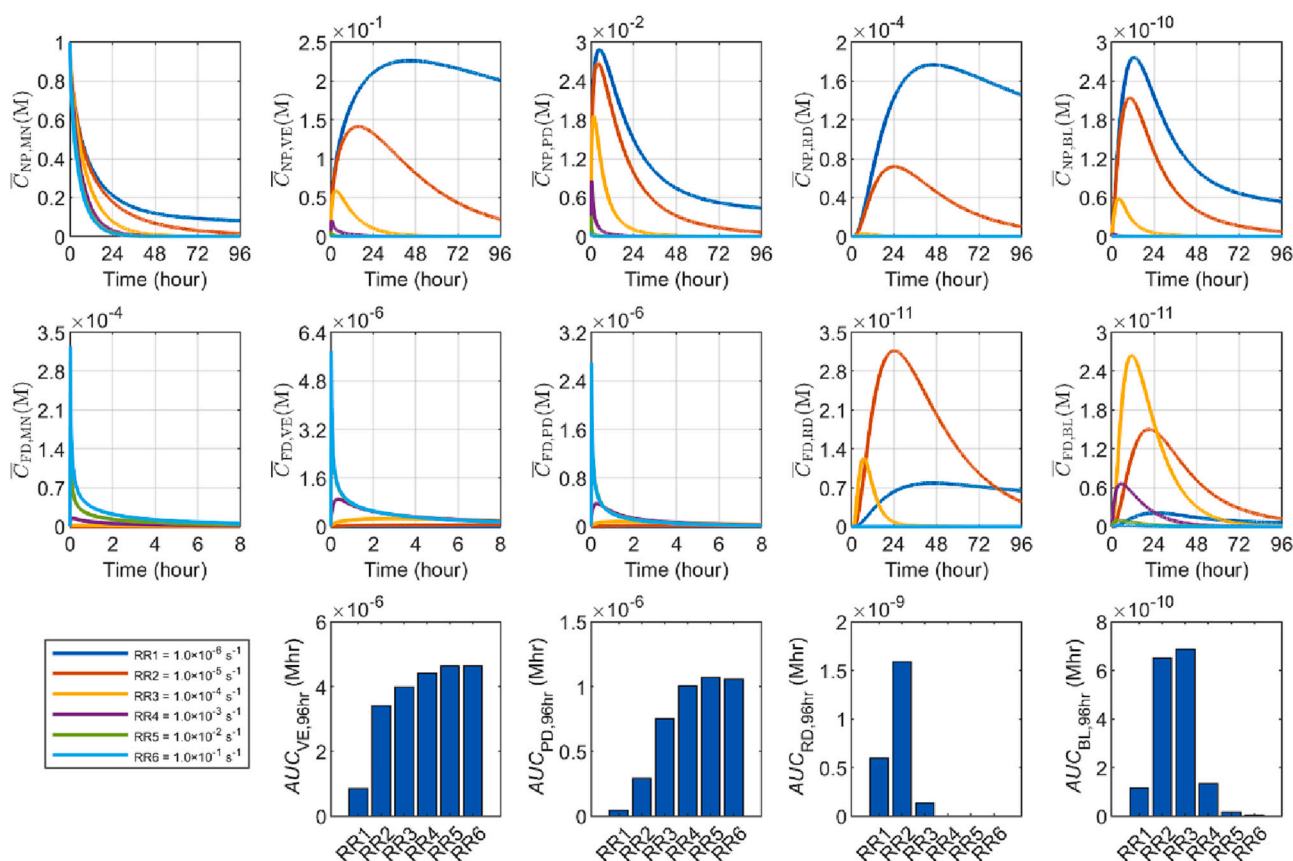
Fig. 6. Comparison of delivery outcomes using nanocarriers with different release rates. Upper panel: time courses of spatial-averaged concentration of nanocarriers; Middle panel: time courses of spatial-averaged concentration of free drugs; Lower panel: exposure to drugs over 96 hours (AUC_{96hr}). The columns represent microneedle (MN), viable epidermis (VE), papillary dermis (PD), reticular dermis (RD) and blood (BL) in turn from left to right.

tissues. This finding indicates that free drugs can efficiently transfer into the microneedle after release, making the microneedle an effective reservoir of free drugs for sustainable drug supply. Moreover, free drugs can accumulate at the microneedle-stratum corneum interface due to the impermeable nature of the stratum corneum.

Fig. 5 shows the spatial-averaged concentration of nanocarriers, free drugs and bound drugs as a function of time in each skin layer and blood. The nanocarrier concentration in the microneedle reduces exponentially as time proceeds due to the continuous transport into the surrounding tissues. In response, the nanocarrier concentration in the viable epidermis rapidly increases to its peak in approximately 3 hours and then gradually decreases. The papillary dermis is the next layer

downstream where the concentration varies in a similar manner. In contrast, the nanocarrier concentrations in the reticular dermis and blood remain at lower levels over time, implying that most drugs accumulate in the upper skin layers of the viable epidermis and papillary dermis. Furthermore, the free drug concentration in the microneedle is significantly higher than in skin tissues and blood. This concentration jumps to its peak around 20 *min* after the treatment starts and then decreases continuously to the near-zero level in about 48 hours. The concentration of free drugs in the viable epidermis and papillary dermis, respectively, show similar trends to that of nanocarriers in the same skin layer. The concentrations of free drugs in the reticular dermis and blood are also greatly lower than in the viable epidermis and papillary dermis,
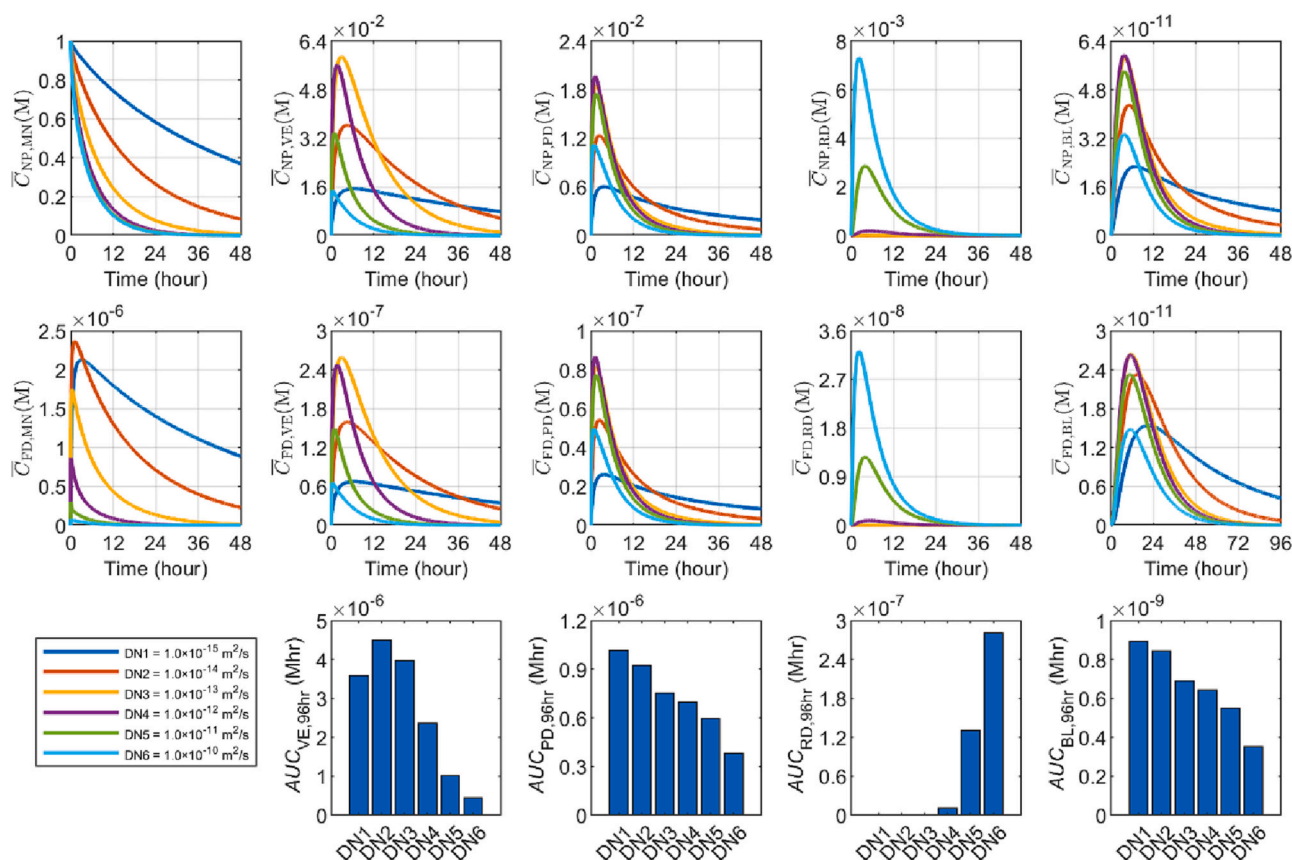
Fig. 7. Comparison of delivery outcomes using nanocarriers with different diffusivity in skin tissue. Upper panel: time courses of spatial-averaged concentration of nanocarriers; Middle panel: time courses of spatial-averaged concentration of free drugs; Lower panel: exposure to drugs over 96 hours (AUC_{96hr}). The columns represent microneedle (MN), viable epidermis (VE), papillary dermis (PD), reticular dermis (RD) and blood (BL) in turn from left to right.

similar to nanocarriers. It is worth noting that, in both the blood and papillary dermis, the bound drug concentration follows a similar trend as the free drug concentration but is 3 times higher, as shown in Fig. 5 (b) and (c). This is because the time window of drug transport is much larger as compared to the rate of drug-protein association and disassociation rates, as indicated by the model parameters in Table 2. Therefore, the following studies will be focused on nanocarriers and free drugs.

3.2. Impact of nanocarrier properties

3.2.1. Nanocarrier release rate

Release rate describes the time scale for nanocarriers to release the payload, with a higher value indicating faster release. As a crucial property that determines the therapeutic activities [43,44], it can vary in a wide range with the formulation, fabrication method and environment [45,46]. The release process of light-responsive nanoparticles may last for a few minutes to hours [47]. Thermosensitive liposomes release the encapsulated drugs in seconds once the environmental temperature rises above a predesigned threshold [48]. In contrast, stealth nanoparticles can provide continuous release over weeks [49]. In order to cover the potential levels that the release rate can reach, the range of $1.0 \times 10^{-6} \sim 1.0 \times 10^{-1}$ s^{-1} [31] is used to examine its impact. The baseline value is 1.0×10^{-4} s^{-1}.

The delivery outcomes of nanocarriers with different release rates are compared in Fig. 6. Results show that increasing the release rate can effectively accelerate the decrease of the nanocarrier concentration in the microneedle, blood and all the layers of skin tissue. This acceleration consequently raises the concentrations of free drugs in the viable epidermis and papillary dermis since more drugs can be released locally.

Microneedle, which is immediately adjacent to the viable epidermis and papillary dermis as shown in Fig. 2, presents a similar trend due to the two-way drug transport between these three compartments. Free drug concentration in the reticular dermis reacts to the change in release rate on a larger time scale. This is because as a downstream layer, all drugs in the reticular dermis are transported from the upstream papillary dermis by diffusion. Although the high release rate enables more free drugs to be released from nanocarriers locally, it also significantly reduces the amount of nanocarriers that can arrive in the reticular dermis, since most drugs are released upstream. As a result, the concentration of free drugs in the reticular dermis exhibits a non-linear relationship with the release rate, with the peak achieved when the rate is 1.0×10^{-5} s^{-1}. A similar response of free drug concentration to release rate can be found in the blood due to the trade-off between the enhancement of local drug release and the reduction in the supply of nanocarriers.

Treatment efficacy is highly sensitive to the release rate, as shown in the lower panel of Fig. 6. Specifically, exposure to drugs in the viable epidermis is positively correlated to the release rate. Increasing the rate from 1.0×10^{-6} s^{-1} to 1.0×10^{-2} s^{-1} can effectively improve the treatment, however, the further increase has less contribution. To be different, the highest AUC in the papillary dermis occurs when the release rate reaches 1.0×10^{-2} s^{-1}. Further accelerating the release dynamics leads to a slight reduction in drug exposure. The best treatment in the reticular dermis can be achieved when the release rate is 1.0×10^{-5} s^{-1}; AUC falls to invisible levels when the release rate is $>1.0 \times 10^{-3}$ s^{-1}, because most drugs deposit in the upper layers of the viable epidermis and papillary dermis. A similar pattern can be found in the blood, where the most effective drug delivery is obtained when the release rate is located in the range of $1.0 \times 10^{-5} \sim 1.0 \times 10^{-4}$ s^{-1}.
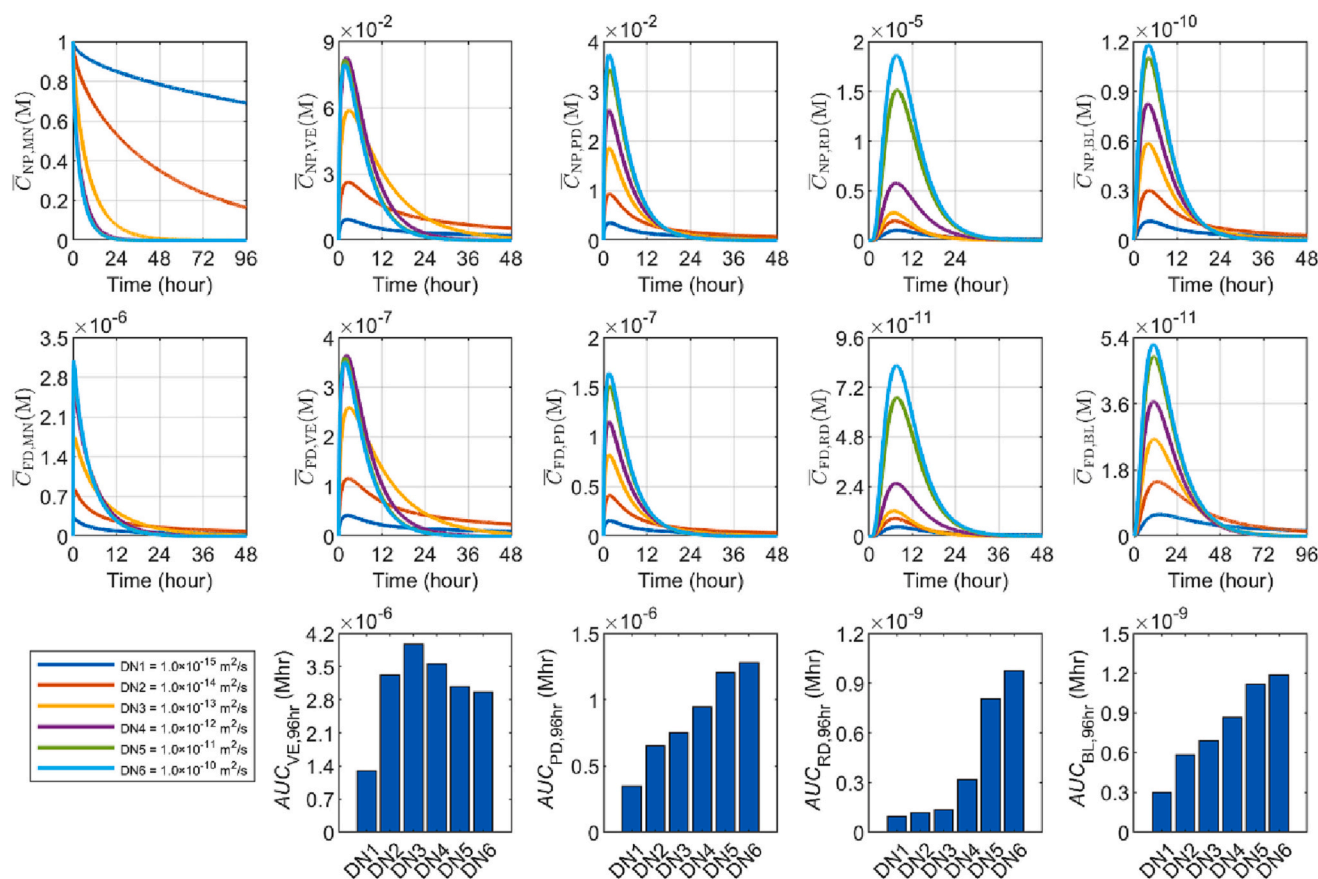
Fig. 8. Comparison of delivery outcomes using nanocarriers with different diffusivity in microneedle. Upper panel: time courses of spatial-averaged concentration of nanocarriers; Middle panel: time courses of spatial-averaged concentration of free drugs; Lower panel: exposure to drugs over 96 hours (AUC_{96hr}). The columns represent microneedle (MN), viable epidermis (VE), papillary dermis (PD), reticular dermis (RD) and blood (BL) in turn from left to right.

3.2.2. Nanocarrier diffusivity in skin tissue

Diffusivity reflects the transport ability of nanocarriers driven by the concentration gradient. It is determined by the properties of the nanocarriers and transport medium, including nanocarrier size, surface charge, environmental temperature, and surrounding interstitial fluid. The diffusivity was measured as 2.4×10^{-13} m^2/s for nanocarriers with a dimension of 100 nm [50], while the parameter of 500 nm nanocarriers decreases to 1.0×10^{-14} m^2/s [51]. For a multistage nanocarrier whose size changes during the delivery process, the diffusivity of 2.3×10^{-11} m^2/s and 2.2×10^{-12} m^2/s were obtained from *in vitro* and *in vivo* experiments [52]. The diffusivity of a 50 nm nanoparticle was reported to be 7.7×10^{-14} m^2/s in cellular microenvironments [53]. In this regard, a large range of $1.0 \times 10^{-15} \sim 1.0 \times 10^{-10}$ m^2/s is applied in this study, with the baseline value of 1.0×10^{-13} m^2/s in Table 2.

Fig. 7 represents the spatial-averaged concentrations of nanocarriers and free drugs as a function of time in different tissue compartments and corresponding drug exposure. Not surprisingly, reducing the nanocarrier diffusivity in tissue slows the loss of nanocarriers from the microneedle due to the deceleration of transport across the microneedle-tissue interface. The peak concentration varies significantly in the viable epidermis and papillary dermis, showing a non-linear relationship with this nanocarrier property. This is because the high diffusivity not only enables more nanocarriers to enter these two skin layers from the microneedle but also allows rapid transport to the downstream layers. Since microvasculature is mainly embedded in the papillary dermis, drug concentrations in the blood and papillary dermis share similar trends. Notably, nanocarriers with lower diffusivity can survival for longer in all compartments except the reticular dermis. This is because higher diffusivity allows more nanocarriers to rapidly travel into the

deep dermis, resulting in fewer nanocarriers remaining in the upper skin layers. Therefore, the concentration in the reticular dermis increases with the nanocarrier diffusivity in the skin tissue. Since all free drugs are released from the nanocarriers, the concentration of free drugs follows similar trends as that of nanocarriers in each layer.

Exposure to drugs (*AUC*) is defined as the integral of drug concentration over time, depending on both the peak concentration and the rate at which the concentration changes with time. Results in the lower panel of Fig. 7 show that the optimal treatment in the viable epidermis takes place when the diffusivity is 1.0×10^{-14} m^2/s, while further increasing the diffusivity leads to a reduction in efficacy. The treatment becomes more effective in the papillary dermis and blood when using nanocarriers with lower diffusivity. However, this is in contrast to the treatment of reticular dermis, in which efficacy is positively correlated to the diffusivity of nanocarriers in tissue.

3.2.3. Nanocarrier diffusivity in microneedle

Diffusive transport of nanocarriers in the microneedle is strongly dependent on the physical and chemical properties of the microneedle and nanocarriers, particularly the formulation. This diffusivity was measured on the scale $10^{-12} \sim 10^{-13}$ m^2/s in polymer gels [54] and $10^{-11} \sim 10^{-13}$ m^2/s in hydrogels [29], respectively. Hence, the range of $1.0 \times 10^{-15} \sim 1.0 \times 10^{-10}$ m^2/s is applied to cover the potential levels this parameter can reach in microneedles; the baseline value is set to be 1.0×10^{-13} m^2/s in Table 2.

Compared in Fig. 8 are the outcomes of transdermal delivery using nanocarriers with different diffusivity in microneedles. It is shown that increasing this diffusivity can effectively accelerate the loss of nanocarriers from the microneedle due to the rapid movement of
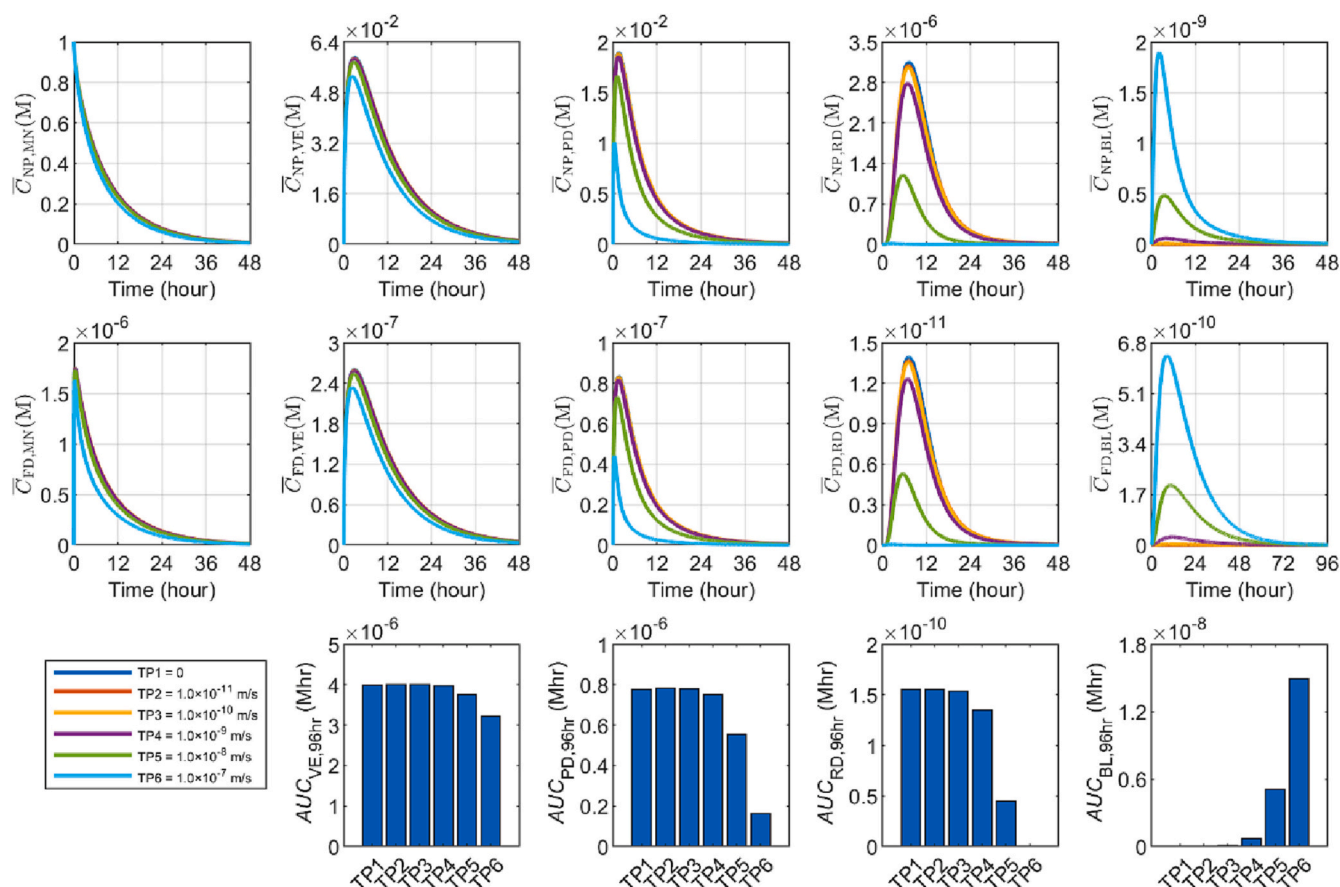
Fig. 9. Comparison of delivery outcomes using nanocarriers with different transvascular permeability. Upper panel: time courses of spatial-averaged concentration of nanocarriers; Middle panel: time courses of spatial-averaged concentration of free drugs; Lower panel: exposure to drugs over 96 hours (AUC_{96hr}). The columns represent microneedle (MN), viable epidermis (VE), papillary dermis (PD), reticular dermis (RD) and blood (BL) in turn from left to right.

nanocarriers towards the microneedle-tissue interface and into the surrounding tissues. This acceleration allows the nanocarrier concentration in all skin layers and the blood to reach a higher peak but fast decrease to a lower level, owing to the unsustainable drug supply from the microneedle. Similar trends can be found for free drugs in each skin layer and blood, demonstrating a direct influence of the nanocarrier concentration on the local concentration of free drugs. Moreover, the optimal treatment in the viable epidermis is achieved when this diffusivity is 1.0×10^{-13} m^2/s. However, the efficacy increases monotonically with this diffusivity in the rest skin layers and blood.

3.2.4. Nanocarrier transvascular permeability

Transvascular permeability stands for the ability of nanocarriers to pass through the capillary wall. Its value is determined by the wall structure and nanocarrier properties, including the formulation and size. On the one hand, capillaries in the skin are nearly impermeable to large molecules due to the continuous basement membrane and tight intercellular clefts [29]. On the other hand, different ligands can be used to modify the surface of nanocarriers, thus enabling the penetrating of the wall of continuous capillaries [55,56]. This parameter was measured in the range of $10^{-11} \sim 10^{-9}$ m/s in experiments [36]. Theoretical analyses further showed that it can be increased to the scale of 10^{-7} m/s when the particle size is reduced to a few nanometres [57]. Therefore, the impact of nanocarrier transvascular permeability is analysed in the range from 0 to 1.0×10^{-7} m/s [31], and the baseline value is 1.0×10^{-9} m/s.

Fig. 9 compares the delivery outcomes of treatments using nanocarriers with different transvascular permeability. The concentration of nanocarriers and free drugs are less influenced in the microneedle and viable epidermis. However, more significant responses can be found in

the papillary dermis and reticular dermis. Nanocarrier transvascular permeability ranging from 0 to 1.0×10^{-9} m/s results in comparable concentrations and drug exposure in these two skin layers, while further raising this parameter can greatly reduce delivery outcomes since more drugs enter the blood. Moreover, drug exposure remains low in the blood until this permeability increases to 1.0×10^{-9} m/s; nanocarrier transvascular permeability greater than this value leads to a sharp increase in drug exposure in blood.

3.2.5. Nanocarrier partition coefficient

Partition coefficient is defined as the ratio of nanocarrier concentration between the skin tissue and microneedle when dynamics equilibrium is reached, depending on the formulations of nanocarriers and microneedles. The partition coefficient between water and octanol was measured in the range from 0.07 to 27.78 in experiments [58,59]. The value of 1.0 is used in the baseline study since the microneedle, such as hydrogel microneedles, can be treated as an aqueous phase like the viable skin tissues [9]. To understand its impact, the partition coefficient of nanocarriers is varied in a range of $0.01 \sim 100$, with an additional extreme case of 0 representing the nanocarriers that can perfectly disperse in the microneedles.

The impact of the nanocarrier partition coefficient on drug concentration and exposure in skin tissues and blood is shown in Fig. 10. Drug concentration remains zero in all skin layers and blood in the extreme situation because no drugs can escape the microneedle. The nanocarrier concentration in the microneedle rapidly decreases when its partition coefficient increases, owing to the improved dispersion ability of nanocarriers in the skin tissues. As a result, nanocarrier concentration in all the downstream compartments can reach a higher peak. However,
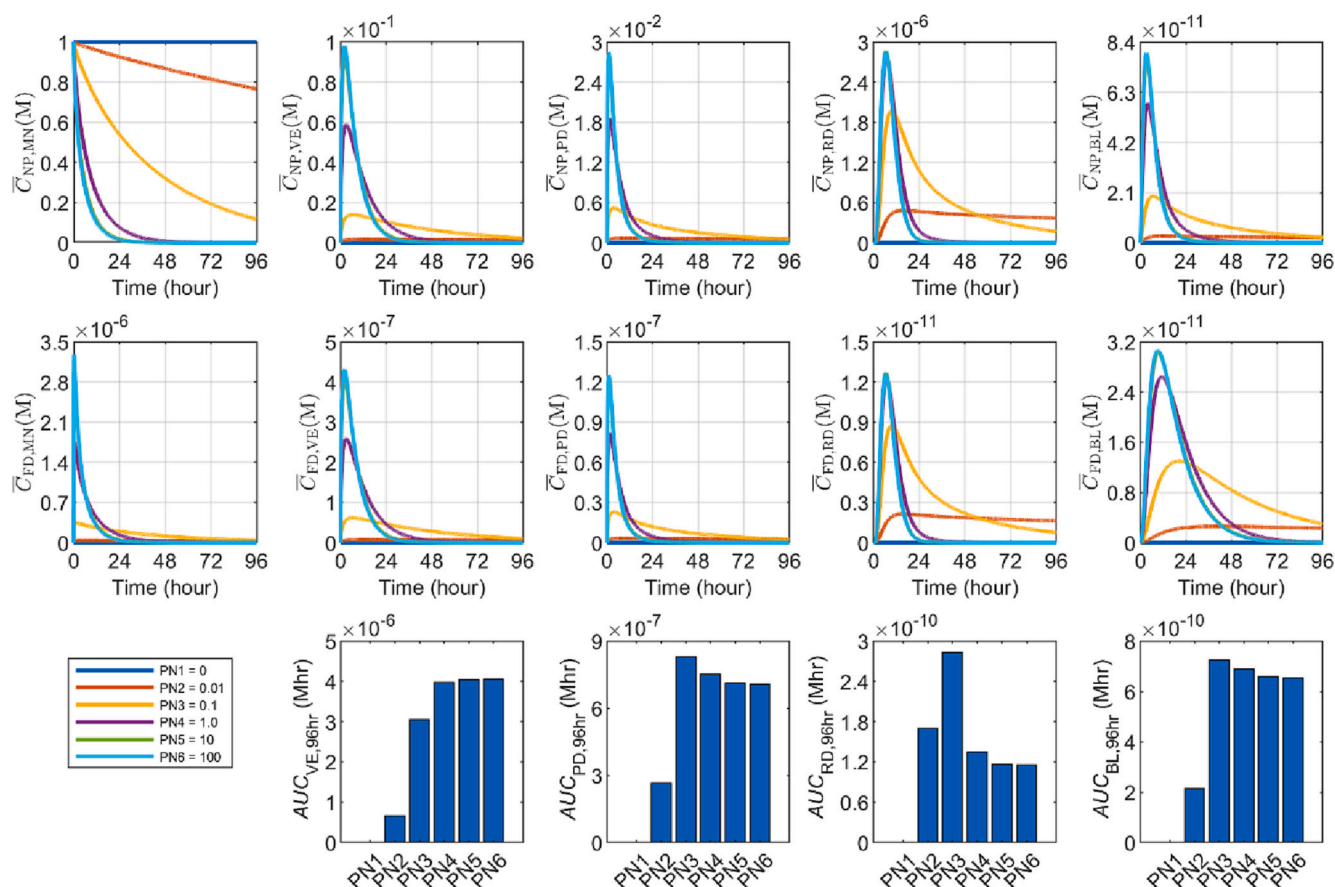
Fig. 10. Comparison of delivery outcomes using nanocarriers with different partition coefficients. Upper panel: time courses of spatial-averaged concentration of nanocarriers; Middle panel: time courses of spatial-averaged concentration of free drugs; Lower panel: exposure to drugs over 96 hours (AUC_{96hr}). The columns represent microneedle (MN), viable epidermis (VE), papillary dermis (PD), reticular dermis (RD) and blood (BL) in turn from left to right.

more drugs can also be eliminated through lymphatic drainage due to the increased concentration, as indicated by Eq. (9). On the contrary, nanocarriers with a lower partition coefficient travel slowly from the microneedle to the tissue, thereby providing a sustainable drug supply over time. Moreover, the concentration of free drugs follows a similar trend as the nanocarrier concentration in each tissue compartment. Since free drugs in the microneedle come from the surrounding skin tissues by diffusion, similar time courses of free drug concentration as in the viable epidermis and papillary dermis can also be found in the microneedle.

Comparisons in the lower panel show that the efficacy in the viable epidermis increases with the partition coefficient; however, the maximum treatment in the papillary dermis, reticular dermis and blood takes place when this partition coefficient is 0.1. This finding demonstrates the significance of optimising the nanocarrier partition coefficient to maintain a balance between high drug concentration and sustained drug supply from the microneedle.

3.3. Impact of microneedle properties

3.3.1. Microneedle length

Length of the microneedle is a factor that can be precisely controlled during fabrication. It directly defines the penetration depth into the skin tissue. This geometrical property is typically on the order of hundreds of micrometres [60,61] and varies in clinical practice to suit specific drug delivery conditions [23]. The design should take into account multiple factors, including the thickness of skin layers, and the location of the target site and administration site, which can differ greatly [22]. The microneedle length is located in the range of 100 μm to 550 μm in this

study to examine its impact on delivery outcomes. Particularly, the 100 μm microneedle stays only in the viable epidermis, while the 550 μm microneedle is sufficiently long to reach the reticular dermis. One should note that the administration dose is calculated as the product of the initial drug concentration in the microneedles and the microneedle volume. Therefore, the radius of the microneedle base, *r* as shown in Fig. 2, is changed simultaneously to keep the dose and initial concentration identical in all the simulations.

The responses of delivery outcomes in each skin layer and blood to the change in microneedle length are given in Fig. 11. The concentration of nanocarriers in the microneedle and viable epidermis decreases more rapidly when the length is increased. This enables fast drug move into the downstream skin layers. A higher concentration peak can be achieved in the papillary dermis and blood when the microneedle is elongated. The most significant enhancement occurs in the reticular dermis when the microneedle is long enough to reach this layer. Similar trends can be found for free drugs in each skin layer and blood. The comparisons on drug exposure in the lower panel show that the efficacy in the viable epidermis reduces with microneedle length, however, using longer microneedles can effectively improve delivery outcomes in the downstream tissue compartments. Particularly, drug exposure in the reticular dermis is dramatically improved when the microneedle can reach this layer.

The microneedle surface at which transdermal delivery begins varies with microneedle length. Shown in Fig. 12 are the surface area (*SA*) of the microneedle in each viable skin layer and the ratio of *SA* to the local tissue volume (*RSV*). The similar positive responses of delivery outcomes, *SA* and *RSV* to the microneedle length in the papillary dermis and reticular dermis demonstrate the importance of microneedle surface
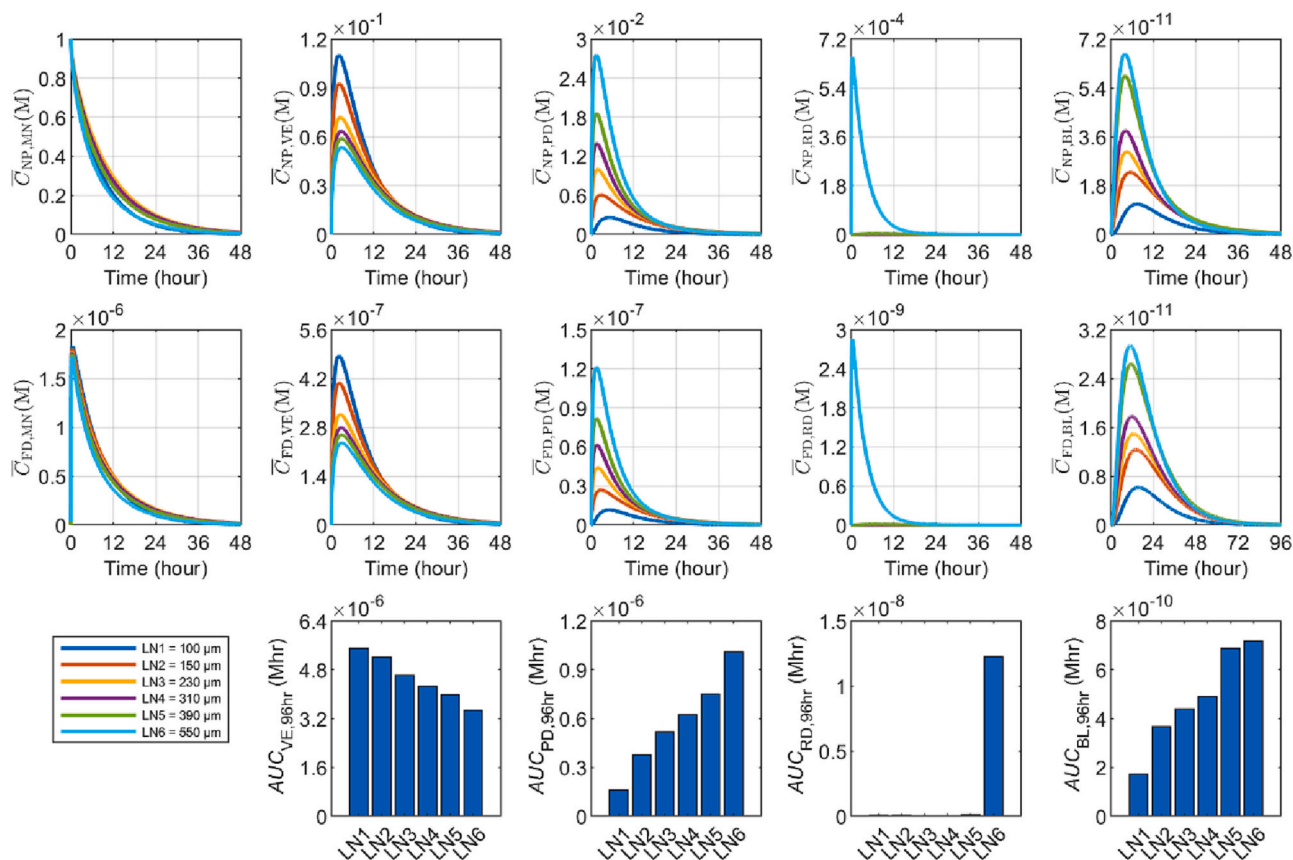
Fig. 11. Comparison of delivery outcomes using microneedles with different heights. Upper panel: time courses of spatial-averaged concentration of nanocarriers; Middle panel: time courses of spatial-averaged concentration of free drugs; Lower panel: exposure to drugs over 96 hours (AUC_{96hr}). The columns represent microneedle (MN), viable epidermis (VE), papillary dermis (PD), reticular dermis (RD) and blood (BL) in turn from left to right.
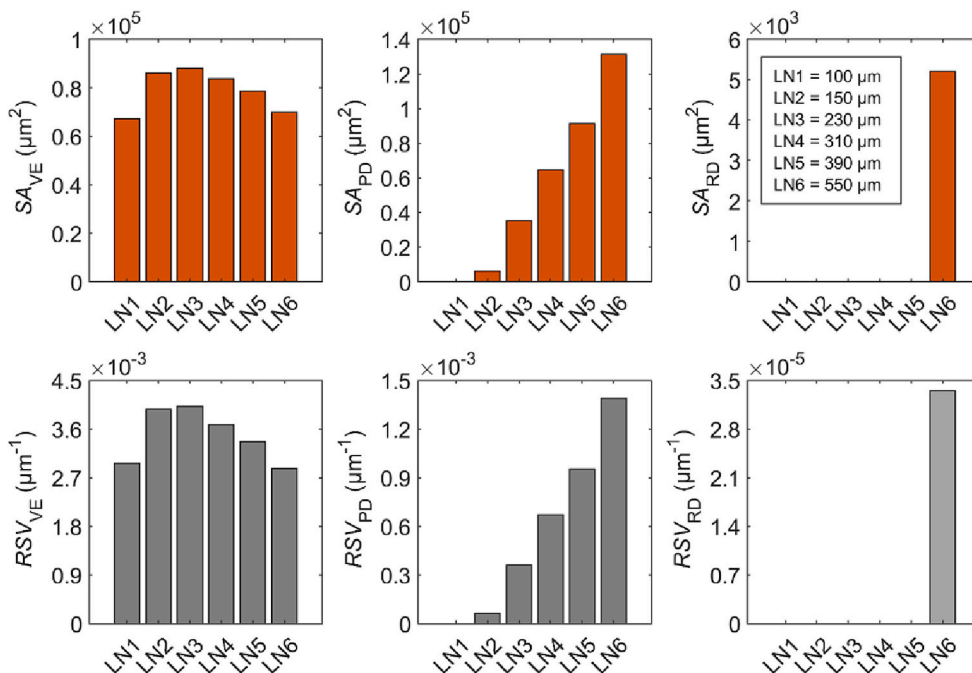
Fig. 12. Comparison of microneedle surface area in viable skin layers (*SA*, upper panel) and the ratio of the surface area to the local tissue volume (*RSV*, lower panel) between the microneedles with different lengths. The columns represent viable epidermis (VE), papillary dermis (PD) and reticular dermis (RD) in turn from left to right.
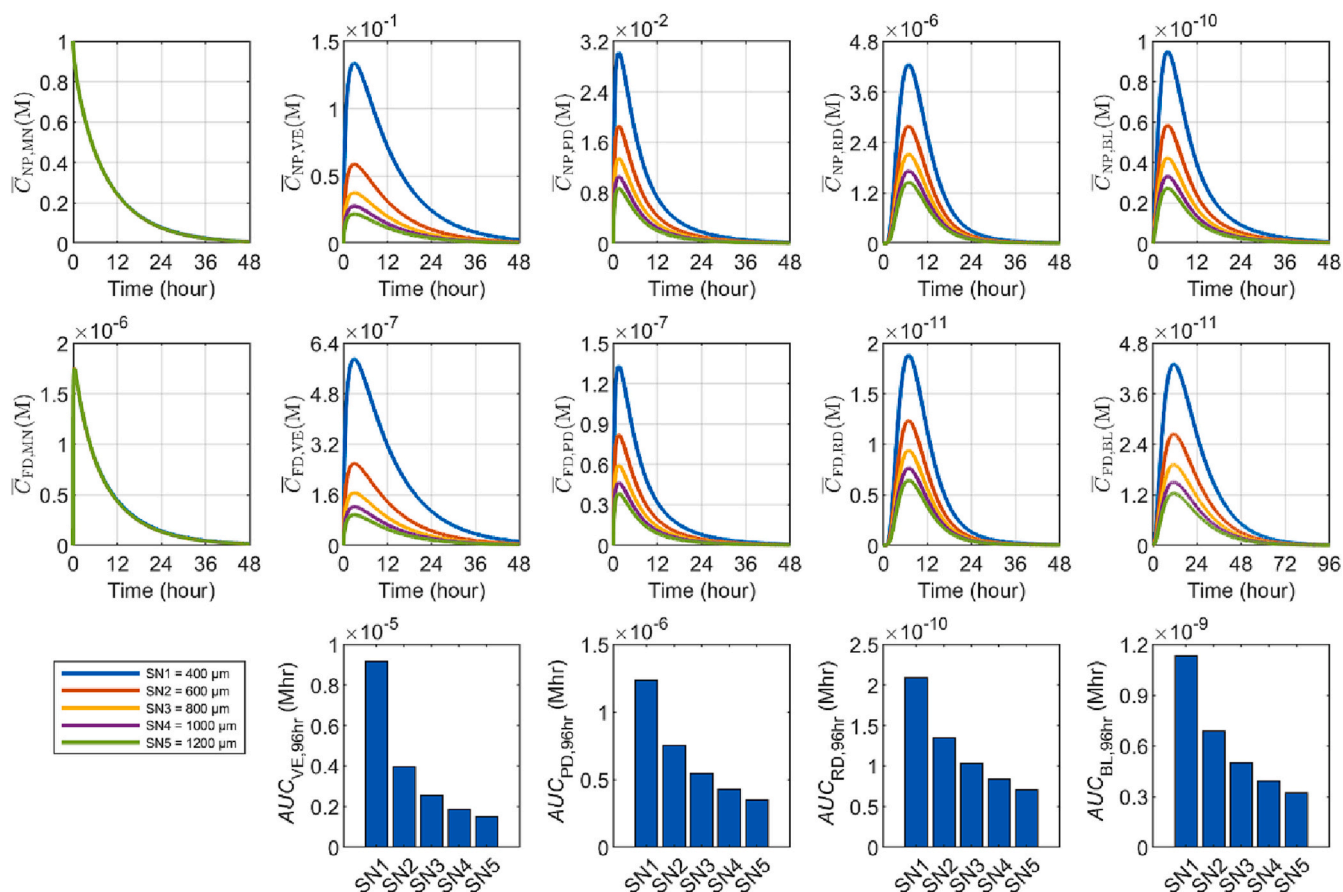
Fig. 13. Comparison of delivery outcomes using microneedles with different spacing. Upper panel: time courses of spatial-averaged concentration of nanocarriers; Middle panel: time courses of spatial-averaged concentration of free drugs; Lower panel: exposure to drugs over 96 hours (AUC_{96hr}). The columns represent microneedle (MN), viable epidermis (VE), papillary dermis (PD), reticular dermis (RD) and blood (BL) in turn from left to right.

area in determining the treatment. Moreover, one should note that although the microneedle with the shortest length of $100\,\mu m$ has a relatively small *SA* and *RSV*, it leads to the most effective drug exposure in the viable epidermis. This is mainly because this microneedle is not long enough to penetrate deep into the papillary dermis and reticular dermis, making the administrated drugs accumulate in the viable epidermis prior to transferring to the deep layers. These results suggest that microneedle surface area and penetration depth are factors that should be considered when choosing to use microneedles with different lengths.

3.3.2. Microneedle spacing

Tip-to-tip distance between microneedles can also be well controlled, determined by the design and manufacturing process. A short distance of $600\,\mu m$ was reported in Ref. [62], and the microneedles are about $1000\,\mu m$ far from each other in Ref. [24]. Therefore, the range of $400 \sim 1200\,\mu m$ is applied in this study. Results summarised in Fig. 13 show that the time courses of spatial-averaged concentration in the microneedle are not sensitive to the change in microneedle spacing. However, increasing this parameter results in a reduction in the drug spatial-averaged concentrations and *AUC* in all the skin tissues and blood. This is because the REV becomes larger due to the increased microneedle spacing, enlarging the volume that each microneedle needs to cover. Quantitative comparisons further reveal an exponential decay relationship between drug exposure and distance between microneedles, suggesting that the most efficient delivery occurs when the microneedles are closely placed on the patch.

3.3.3. Diffusivity of free drugs in microneedle

Diffusivity of free drugs describes the transport ability of small molecule drugs in the microneedle due to thermal motion, subject to the drug molecules and transport medium. This diffusivity of the selected representative drug doxorubicin in hydrogel was reported to be $8.2 \times 10^{-10} \sim 2.34 \times 10^{-9}\,m^2/s$ [30]. This parameter in polymers with different formulations ranged from $1.85 \times 10^{-11}\,m^2/s$ to $1.18 \times 10^{-10}\,m^2/s$ [63]. Therefore, a board range from $1.0 \times 10^{-12}\,m^2/s$ to $1.0 \times 10^{-8}\,m^2/s$ is used in this study to examine its impact on delivery outcomes; the baseline value of $1.0 \times 10^{-10}\,m^2/s$ is applied in Table 2. Results in Fig. 14 show that increasing this diffusivity can slightly raise the peak concentration of free drugs in the microneedle. However, drug concentration and drug exposure in all skin layers and blood are not sensitive to the changes in this property.

3.3.4. Partition coefficient of free drugs

Partition coefficient of free drugs is defined as the ratio of free drug concentration between the surrounding skin tissues and microneedle when dynamic equilibrium is reached. It depends on the properties of small molecule drugs, and transport media of tissue and microneedle. The partition coefficient between water and octanol was found to be 17.85 [64] and 20.83 [65]. The value is set as 1.0 in the baseline study for the microneedles that can be treated as an aqueous phase as the viable skin tissues [9]. Hence, a range of $0 \sim 100$ is adopted to cover the possible values of this parameter, reflecting the influence introduced by the microneedle materials. The extreme case of 0 refers to the microneedles in which free drugs can perfectly disperse.

The impact of the partition coefficient of free drugs in microneedles on delivery outcomes is shown in Fig. 15. Results demonstrate that the
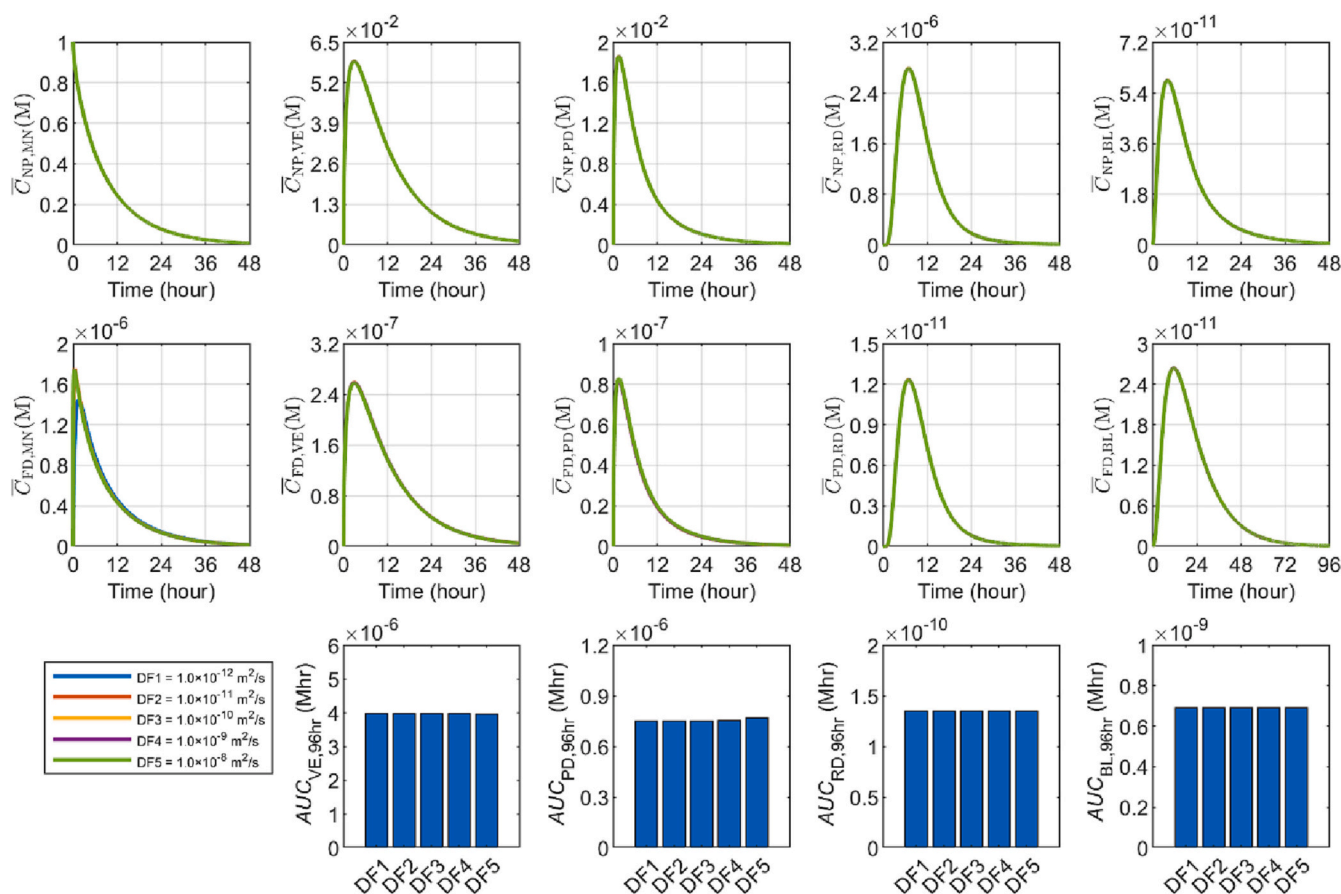
Fig. 14. Comparison of delivery outcomes using microneedles where free drugs have different diffusivity. Upper panel: time courses of spatial-averaged concentration of nanocarriers; Middle panel: time courses of spatial-averaged concentration of free drugs; Lower panel: exposure to drugs over 96 hours (AUC_{96hr}). The columns represent microneedle (MN), viable epidermis (VE), papillary dermis (PD), reticular dermis (RD) and blood (BL) in turn from left to right.

concentration of nanocarriers remains the same no matter how this partition coefficient varies. Making the microneedle more dispersible to small-molecule drugs can effectively improve free drug accumulation in the microneedle and cause a slight reduction in the concentration in the viable epidermis and papillary dermis. However, the responses in the reticular dermis and blood are neglectable. This finding suggests that drug exchange between microneedles and tissue is less decisive for delivery outcomes in the skin tissue and blood.

3.3.5. Physical degradation rate of free drugs in microneedle

Physical degradation rate describes the time scale of drug elimination in the microneedle due to changes to materials resulting from ambient conditions. It is strongly affected by the properties of the microneedle, including the formulation and microstructure. For instance, experiments showed that polymer can protect the loaded drugs from degradation as compared to phosphate-buffered saline [66]. To examine how this factor influences delivery outcomes, the baseline value in Table 2 is varied in a range of $0 \sim 100$ fold for an exploratory parametric study. As the delivery outcomes shown in Fig. 16, no significant differences can be found for the drug concentrations in all the skin layers, blood and even microneedle. Therefore, the drug accumulation in the microneedle is more dominated by diffusion, as indicated by Eq. (6). The modelling predictions show that this factor has a fairly low impact which can be ignored.

3.3.6. Loading dose

Drugs are loaded in microneedles in the nanocarrier-encapsulated form. Influenced by the microneedle formulation, the loading dose is a precisely controllable parameter in practice. The baseline value in

Table 2 is varied in the range of $0.1 \sim 10$ fold to examine its effects. The delivery outcomes in treatment using different loading doses are given in Fig. 17. The nanocarrier concentration and free drug concentration increase proportionally with the loading dose in all compartments since more drugs are administrated. Qualitative analyses also demonstrate that drug exposure varies in proportion to the loading dose, as shown in the lower panel.

3.4. Impact of environment

3.4.1. Air velocity

Air velocity, or wind speed, directly determines the TEWL rate and further influences the interstitial fluid flow in skin tissues. It is commonly judged using the Beaufort scale [67], on which the air velocity of calm, fresh breeze and violent storm are $0 \sim 0.45$ m/s, $8.50 \sim 10.73$ m/s and $28.6 \sim 32.2$ m/s, respectively. To focus on the environment in daily life, the range of $0 \sim 10.0$ m/s is selected in this study.

Fig. 18 compares interstitial fluid velocity in each skin layer at the delivery conditions of different air velocities. Results show that the interstitial fluid flow is accelerated in all skin layers with the increase in the air velocity since stronger wind leads to faster water loss to the environment from the skin surface. Its influence on drug delivery is represented in Fig. 19. Drug accumulation in the viable epidermis is improved when the wind is strong. However, the concentrations decrease with the air velocity in the papillary dermis, reticular dermis and blood. This is because the interstitial fluid flows from the deep skin layers to the skin surface, as shown by the vectors in Fig. 3, which is opposite to the direction of drug diffusion. Hence, more drugs would accumulate in the viable epidermis due to enhanced convective
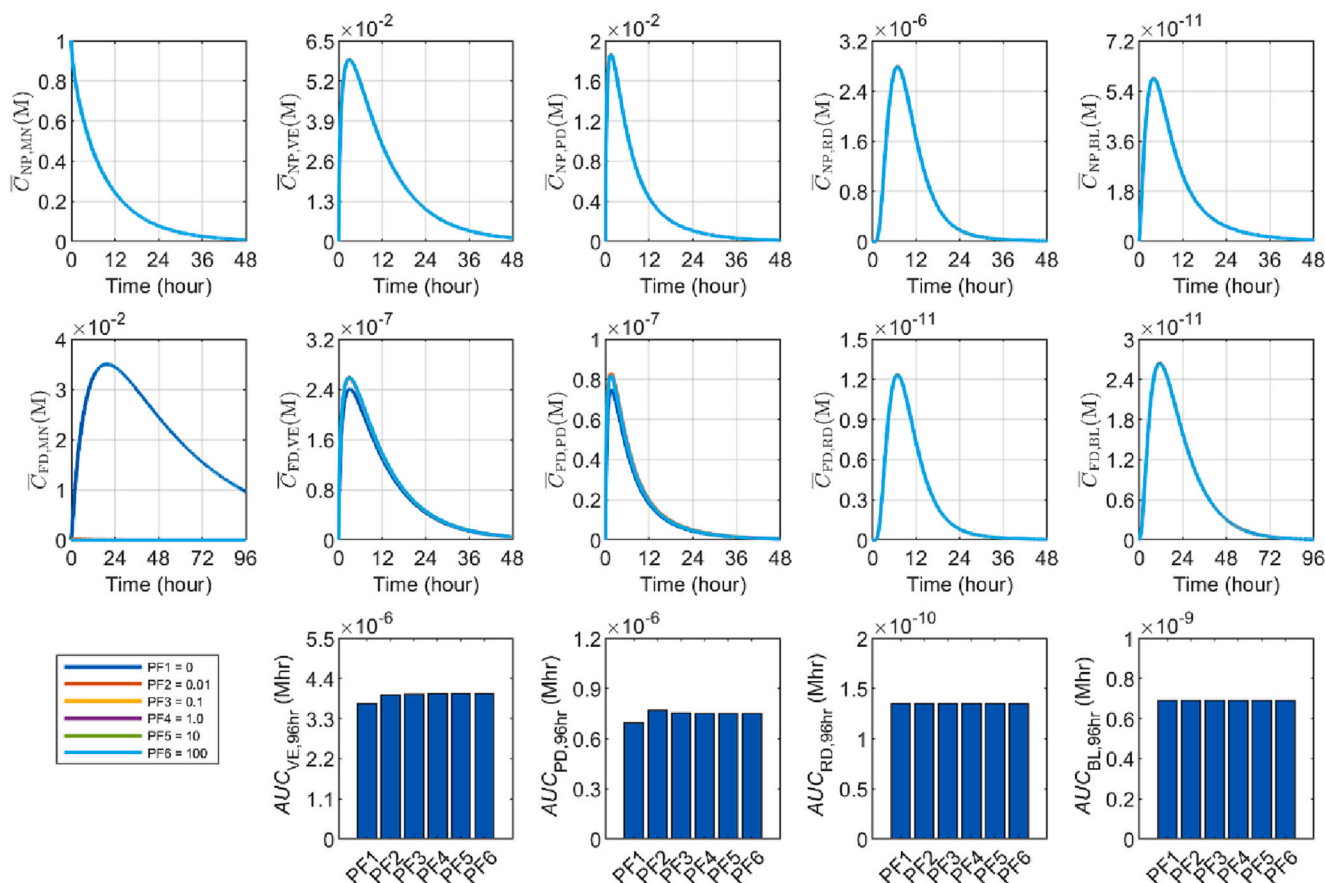
Fig. 15. Comparison of delivery outcomes using microneedles with different partition coefficients of free drugs. Upper panel: time courses of spatial-averaged concentration of nanocarriers; Middle panel: time courses of spatial-averaged concentration of free drugs; Lower panel: exposure to drugs over 96 hours (AUC_{96hr}). The columns represent microneedle (MN), viable epidermis (VE), papillary dermis (PD), reticular dermis (RD) and blood (BL) in turn from left to right.

transport in this skin layer. On the contrary, the delivery to deep skin layers becomes less effective as a result of the raised local resistance to drug transport. Given that all drugs in the blood are from the papillary dermis, the drug concentrations in these two compartments share similar trends. Therefore, drug exposure in the viable epidermis can be enhanced when the wind becomes strong, whereas efficacy in rest skin layers and blood presents a negative relationship with air velocity, as shown in the lower panel of Fig. 19.

3.4.2. Relative humidity

Relative humidity is another environmental factor that can directly affect TEWL, ranging from 0 to 100%. Its impact on the interstitial fluid flow is shown in Fig. 20. The relative humidity raising from 0 to 80% results in a gradual decrease in the interstitial fluid velocity; a sharp fall occurs when it is higher than 80%.

Fig. 21 shows the delivery outcomes under the conditions of different relative humidity. No significant difference can be found when the relative humidity changes in the range of 0 ~ 80%. Further increasing it to 100% causes a reduction in drug concentration and drug exposure in the viable epidermis. However, the delivery to the rest compartments is slightly improved. This can also be attributed to the opposite directions of interstitial fluid flow and drug diffusion. Slow interstitial fluid flow allows more drugs to transfer into the deep tissue, thereby increasing the drug concentration in the papillary dermis, reticular dermis and blood. Consequently, few drugs are left in the upstream layer of the viable epidermis.

4. Discussion

Microneedles can directly deliver the loaded drugs into skin tissues by piercing the stratum corneum. Compared to routine topical and transdermal delivery in which drugs are administrated on the skin surface, microneedles can dramatically improve drug accumulation in all skin layers and blood [8,25]. This is because of the nearly impermeable nature of the stratum corneum, which features one of the major barriers protecting the body from external substances.

Responses of delivery outcomes to the changes in the properties of microneedle-nanocarrier combined DDS and environmental factors differ greatly between each skin layer and blood, due to the complex interplays among the tissue, DDS and environment. These variations highlight the demand for tailoring the design and fabrication of microneedles and nanocarriers with optimal properties for specific clinical applications, particularly taking into account the location of the target site. For instance, the use of short microneedles and fast-release nanocarriers facilitates localised drug delivery in the viable epidermis. This would allow for a more precise treatment to minimise the risks of side effects. A major application of this combined DDS in transdermal delivery is efficiently sending drugs to deep skin tissues such as the reticular dermis. Using microneedles that are long enough to reach the target layer can be one of the most immediate solutions. The effectiveness can also be improved by using small nanocarriers [52] that can diffuse rapidly in microneedles and skin tissue. In addition, the influence of the environment should also be considered. Drug delivery to deeper skin layers can be enhanced by reducing wind speed and increasing relative humidity. These require a specific design to make the microneedle patch more windproof and moisturizing. Drug delivery to the circulatory
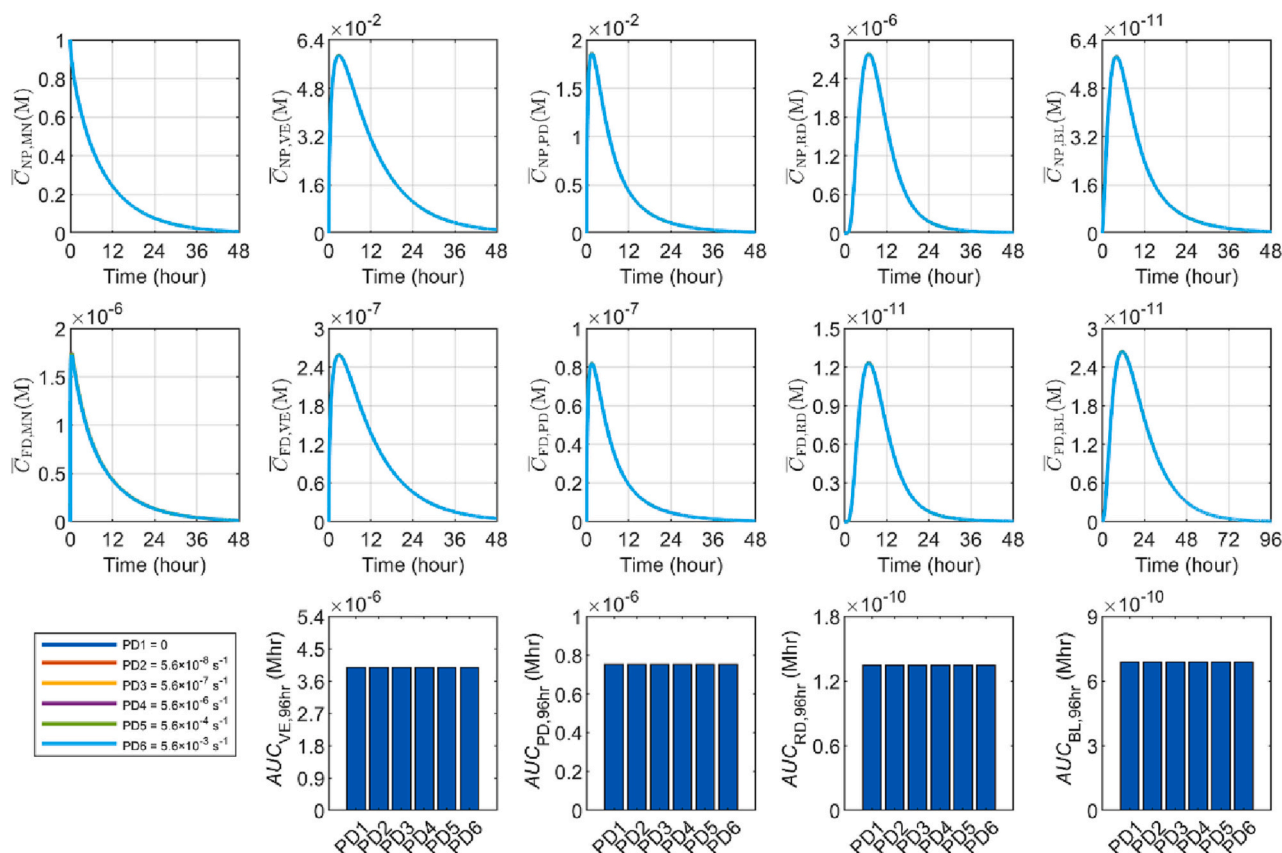
Fig. 16. Comparison of delivery outcomes using microneedles where free drugs have different rates of physical degradation. Upper panel: time courses of spatial-averaged concentration of nanocarriers; Middle panel: time courses of spatial-averaged concentration of free drugs; Lower panel: exposure to drugs over 96 hours (AUC_{96hr}). The columns represent microneedle (MN), viable epidermis (VE), papillary dermis (PD), reticular dermis (RD) and blood (BL) in turn from left to right.

system is another major application. Increasing the loading dose and optimising the partition coefficient of nanocarriers are effective ways to improve. However, attention should also be paid to the possibility of simultaneously increasing drug exposure to other skin layers. Among the influencing factors examined in this study, raising the nanocarrier transvascular permeability is the only way to increase drug concentrations in blood while keeping skin tissue drug exposure low. Since capillaries in skin tissue are continuous with no large gaps that allow macromolecules to pass through the vessel wall, surface modification of nanocarriers with certain ligands may be important [56,68].

The mathematical model in this study is developed to simulate transdermal drug delivery. The modelling predicted distance courses of the concentration of 8-methoxypsoralen and hydrocortisone are compared with experimental measurements in Fig. 22(a) and (b), respectively, with the simulations carried out under the same conditions as in Ref. [15]. The coefficients of determination are calculated as 0.85 and 0.87, demonstrating the good agreement between the modelling and experiments. Mathematical modelling has been broadly applied in research in drug delivery. Several studies have validated the predictive power [69–71]. For instance, the infusion of Evans blue and albumin into agarose gel was modelled in Ref. [72] using a tissue-scale drug delivery model. The coefficients of determination between the predictions and experiments were found to be 0.70 and 0.83, respectively. However, it is important to mention that the predictions of mathematical modelling on drug concentration and distribution remain qualitative. This is because, on the one hand, the modelling requires a large number of parameters whose values are time and location dependent, more importantly, vary greatly between patients. Due to the difficulties to get the full set of model parameters for each patient, representative values obtained from different sources are commonly used. On the other

hand, drug delivery processes *in vivo* are complex. Mathematical models are established to catch the key processes while some of the processes are either ignored or lumped with the key processes, thus reducing the prediction accuracy. Despite these limitations, the modelling predictions are sufficient to provide qualitative trends of delivery outcomes under given conditions for comparison. Findings from this study allow for understanding the importance of each factor and identifying the opportunities for improving delivery outcomes. The modelling accuracy can be increased by developing mathematical models of specific delivery processes with the support of biochemical and physiological studies and measuring model parameters from *in vivo* experiments and medical images.

There are some assumptions involved in this study. (1) The representative values of skin tissue properties are applied. However, the values can vary in a large range depending on the location and patient, particularly the thickness of each skin layer. As a result, the microneedle with a length of 550 μm may not be long enough to reach the reticular dermis in all situations. The length of microneedles needs to be re-determined when the thicknesses of skin layers change. Future studies can also be focused on the impact of different skin tissue properties to develop advanced DDS for transdermal drug delivery at a specific location of the body. (2) Temperature is an environmental factor that can play a key role in transdermal delivery. It will not only influence the drug diffusivity due to molecule thermal motion but also alter the blood perfusion in the skin tissue. Temperatures below the lower end of the thermoneutral zone lead to the closure of arteriovenous anastomoses, in which small arteries and small veins are directly connected [73]. This bypass of capillaries will consequently change the interstitial fluid flow and drug transport to the circulatory system. However, since there is a lack of a mathematical model to precisely describe these processes, the
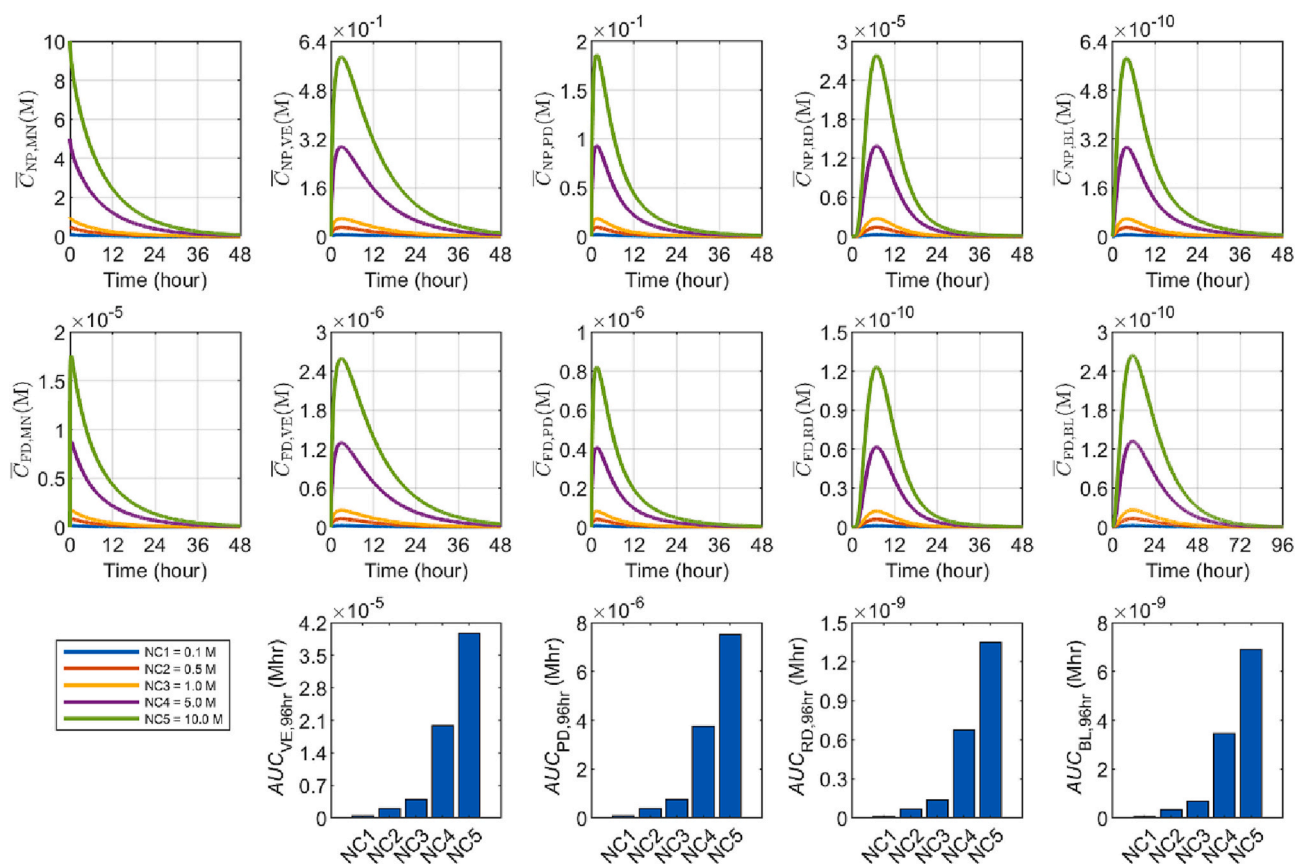
Fig. 17. Comparison of delivery outcomes using microneedles with different administration doses. Upper panel: time courses of spatial-averaged concentration of nanocarriers; Middle panel: time courses of spatial-averaged concentration of free drugs; Lower panel: exposure to drugs over 96 hours (AUC_{96hr}). The columns represent microneedle (MN), viable epidermis (VE), papillary dermis (PD), reticular dermis (RD) and blood (BL) in turn from left to right.
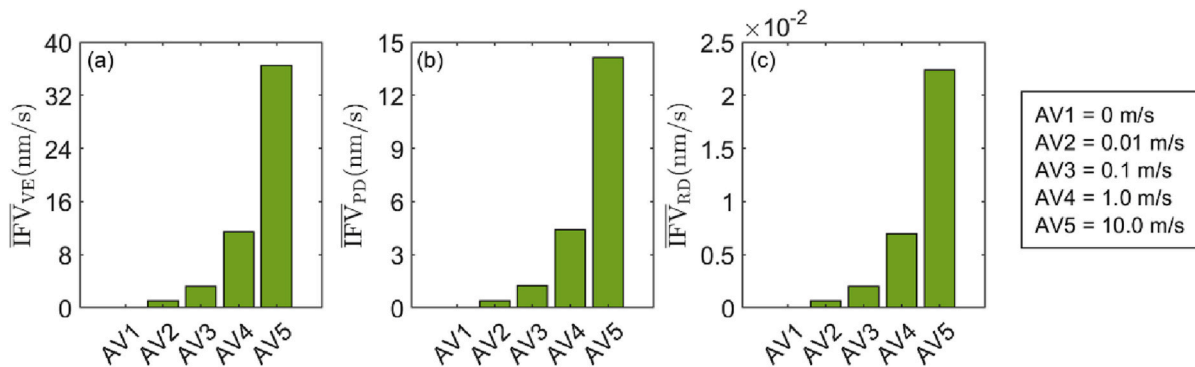
Fig. 18. Comparison of spatial-averaged interstitial fluid velocity ($\overline{IFV}$) in skin layers under environmental conditions with different air velocities.

impact of temperature is not discussed in this study. Results from physiological studies will be needed to establish the relationship between environmental temperature, blood perfusion and arteriovenous anastomoses closure. This relationship can be further combined with the model in this study to examine the role of temperature. (3) The conical microneedles are selected in this study. This allows the model geometry to be simplified to a 2D axis-symmetric configuration, as shown in Fig. 2 (c), for a comprehensive parametric analysis with affordable computational resources. It is worth noting that the shape of microneedles varies greatly depending on the materials and fabrication techniques, such as pyramid-shaped microneedles, pencil-shaped microneedles, and arrow-shaped microneedles [74,75]. The mathematical model developed in this study can be further applied to predict the drug delivery outcomes

using these microneedles while accommodating their geometry in 3D. (4) A general microneedle and nanocarrier are used without specifying the formulation and type. This enables the exploratory parametric studies to examine the impact of different microneedle and nanocarrier properties. Please note that although the models of interstitial fluid flow and drug transport in the skin tissue have certain degrees of generality, the model used in this study needs to be developed to examine the delivery using a specific type of microneedle or nanocarrier to accommodate their unique features. For instance, the microneedle-tissue interface needs to be tracked when studying dissolving microneedles. A pressure-driven fluid infusion model is required for simulating drug delivery using hollow microneedles. (5) In order to focus on the properties of the DDS including the microneedle and nanocarriers, the properties of small
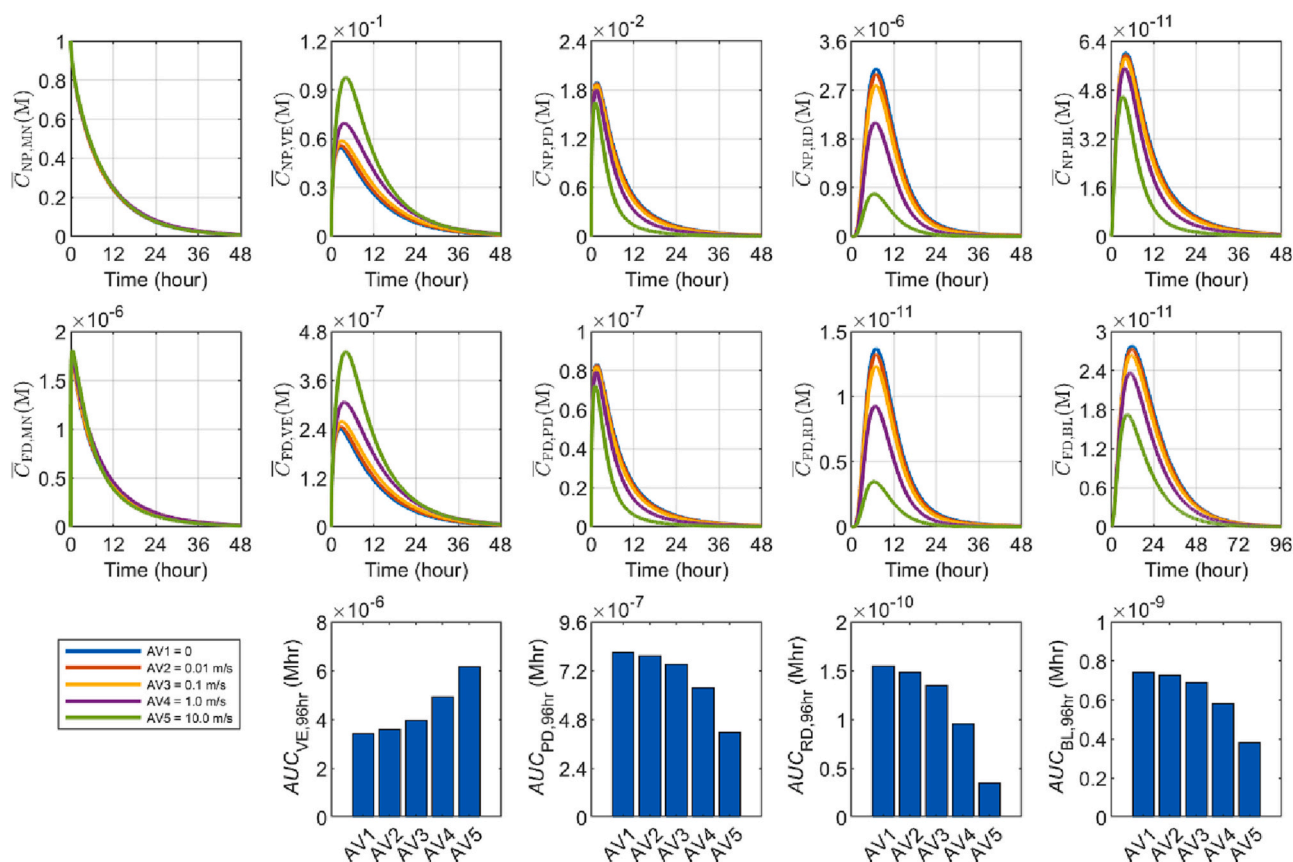
Fig. 19. Comparison of delivery outcomes under different air velocities. Upper panel: time courses of spatial-averaged concentration of nanocarriers; Middle panel: time courses of spatial-averaged concentration of free drugs; Lower panel: exposure to drugs over 96 hours (AUC_{96hr}). The columns represent microneedle (MN), viable epidermis (VE), papillary dermis (PD), reticular dermis (RD) and blood (BL) in turn from left to right.
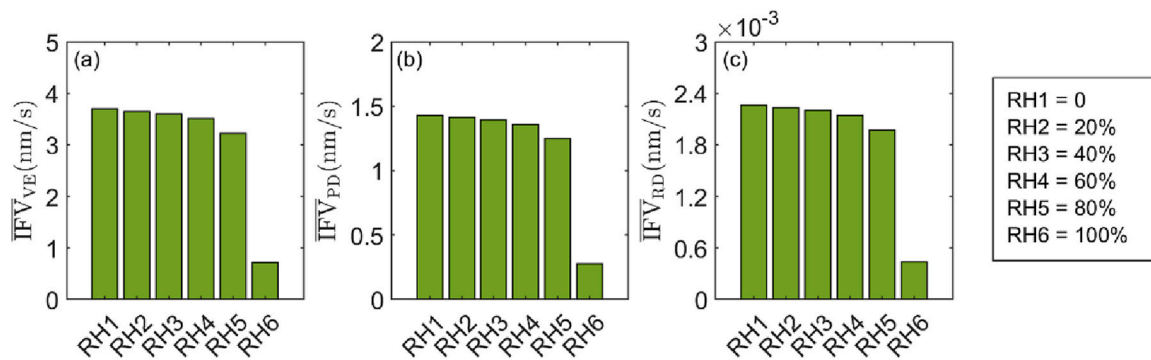
Fig. 20. Comparison of spatial-averaged interstitial fluid velocity ($\overline{IFV}$) in skin layers under environmental conditions with different relative humidity.

molecule drugs in the skin tissue and blood are kept identical in all simulations. A follow-up study can be carried out to examine the performance of different drugs for drug selection and DDS optimisation.

5. Conclusions

Microneedle-mediated delivery of nanocarrier-encapsulated drugs to skin tissues and blood has been studied under various delivery conditions. The results demonstrate that microneedles can effectively deliver drugs to viable skin tissues by penetrating the stratum corneum. Delivery outcomes in skin layers and blood differ significantly with the changes in microneedle properties, nanocarrier properties and environmental factors, but are less sensitive to the changes in free drug

properties induced by the microneedle formulation. Specifically, the release rate should be optimised to maximise drug exposure in the papillary dermis, reticular dermis and blood, while efficacy in the viable epidermis increases with release rates. Increased nanocarrier diffusivity in tissues leads to a reduction in drug exposure in the papillary dermis and blood but enhanced delivery in the reticular dermis; whereas treatment in these three compartments can all be improved by increasing the nanocarrier diffusivity in microneedles. On the other hand, optimisation is required for these two diffusion coefficients for better treatment in the viable epidermis. Likewise, the nanocarrier partition coefficient needs to be determined individually for each skin layer according to the location of the target site. Raising the transvascular permeability of nanocarriers can effectively improve the
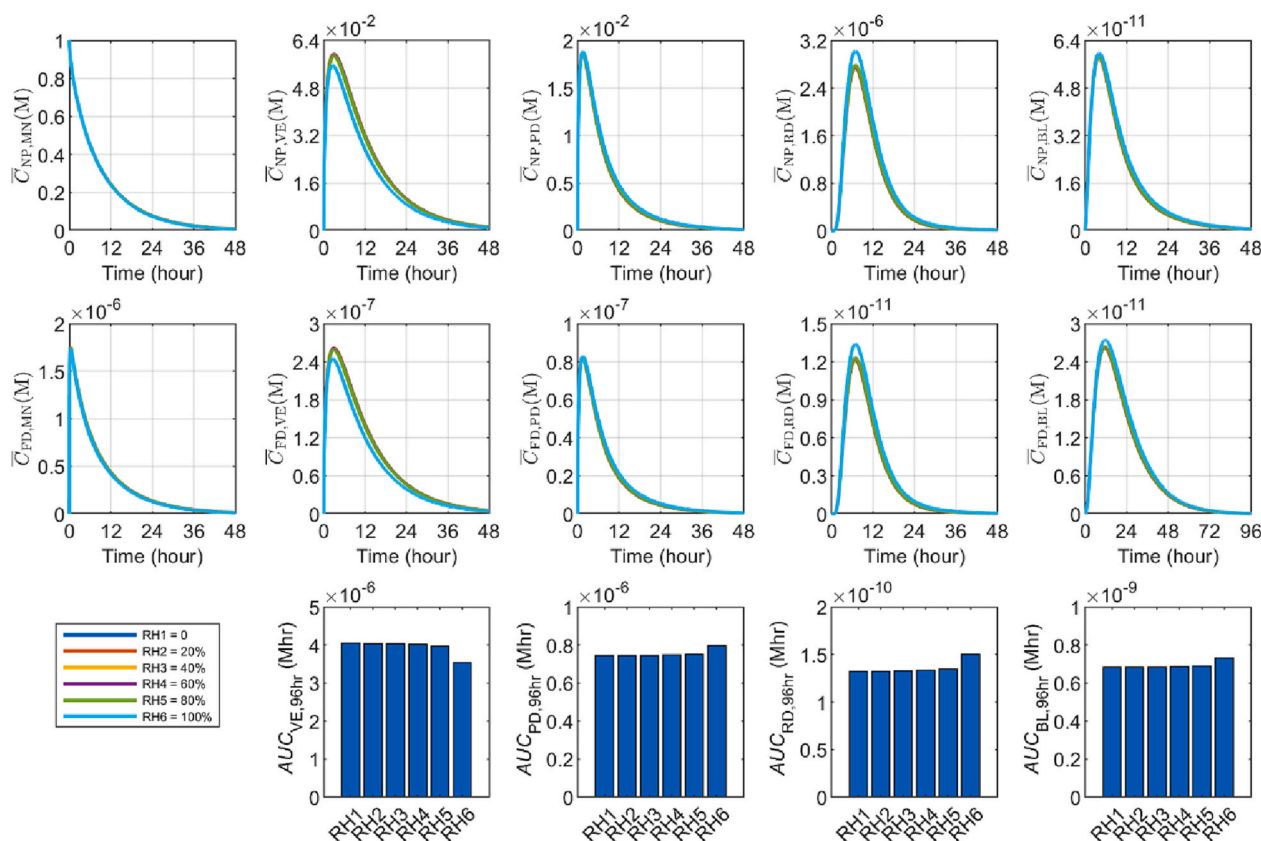
Fig. 21. Comparison of delivery outcomes under different relative humidity. Upper panel: time courses of spatial-averaged concentration of nanocarriers; Middle panel: time courses of spatial-averaged concentration of free drugs; Lower panel: exposure to drugs over 96 hours (AUC_{96hr}). The columns represent microneedle (MN), viable epidermis (VE), papillary dermis (PD), reticular dermis (RD) and blood (BL) in turn from left to right.
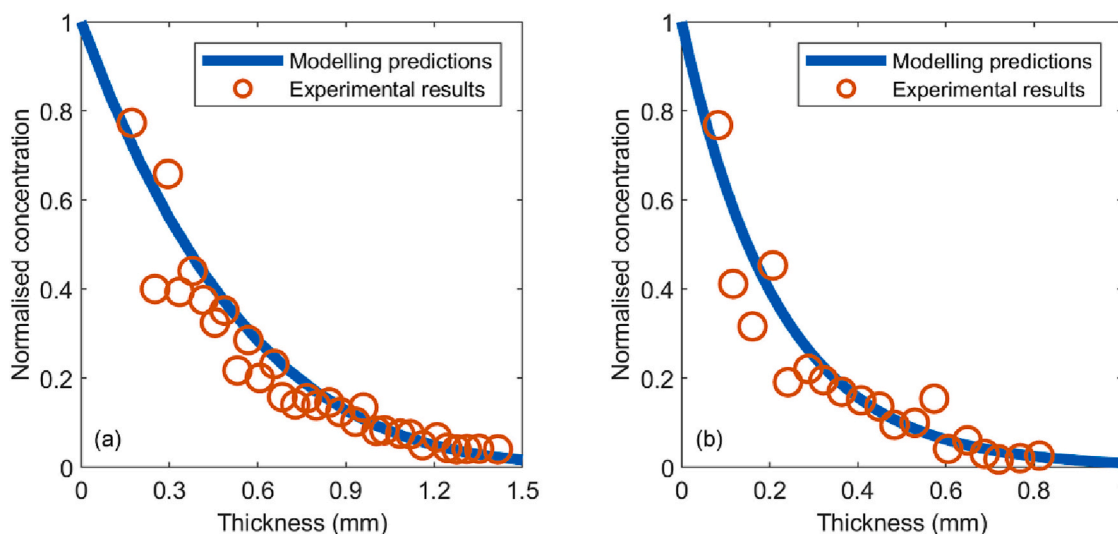
Fig. 22. Comparison of modelling predictions with experimental measurements of 8-methoxypsoralen (a) and hydrocortisone (b) concentration as a function of depth into the dermis. Experimental data and model parameters are extracted from Ref. [15].

delivery to the blood while reducing drug exposure in skin layers. Moreover, better treatment in all skin layers and blood can be achieved by reducing the microneedle spacing and raising the loading dose. Elongating microneedles can effectively enhance drug delivery to deep tissues and blood, especially the reticular dermis; however, the efficacy may be reduced in the viable epidermis. The environment also plays a role. Drug exposure in the viable epidermis increases with increasing wind speed and decreasing relative humidity. The opposite trends can be found in the papillary dermis, reticular dermis and blood. The results obtained from this study can serve as a reference for improving the design of this microneedle-nanocarrier combined drug delivery system and developing transdermal drug delivery regimes.

CRediT authorship contribution statement

Ben Newell: Writing – original draft, Methodology, Investigation, Formal analysis. **Wenbo Zhan:** Writing – review & editing, Investigation, Conceptualization.

Declaration of Competing Interest

The authors have declared that no competing interests exist.

Data availability

Data will be made available on request.

References

[1] S. Bajaj, A. Whiteman, B. Brandner, Transdermal drug delivery in pain management, Contin. Educ. Anaesthesia, Crit. Care Pain 11 (2011) 39–43, https://doi.org/10.1093/bjaceaccp/mkq054.

[2] X. Zhan, G. Tang, S. Chen, Z. Mao, A new copolymer membrane controlling clonidine linear release in a transdermal drug delivery system, Int. J. Pharm. 322 (2006) 1–5, https://doi.org/10.1016/j.ijpharm.2006.05.031.

[3] O. Rascol, S. Perez-Lloret, Rotigotine transdermal delivery for the treatment of Parkinson's disease, Expert. Opin. Pharmacother. 10 (2009) 677–691, https://doi.org/10.1517/14656560902746041.

[4] H. Benson, Transdermal drug delivery: Penetration enhancement techniques, Curr. Drug Deliv. 2 (2005) 23–33, https://doi.org/10.2174/1567201052772915.

[5] M.R. Prausnitz, S. Mitragotri, R. Langer, Current status and future potential of transdermal drug delivery, Nat. Rev. Drug Discov. 3 (2004) 115–124, https://doi.org/10.1038/nrd1304.

[6] A.S. Rzhevskiy, T.R.R. Singh, R.F. Donnelly, Y.G. Anissimov, Microneedles as the technique of drug delivery enhancement in diverse organs and tissues, J. Control. Release 270 (2018) 184–202, https://doi.org/10.1016/j.jconrel.2017.11.048.

[7] R. Goyal, L.K. Macri, H.M. Kaplan, J. Kohn, Nanoparticles and nanofibers for topical drug delivery, J. Control. Release 240 (2016) 77–92, https://doi.org/10.1016/j.jconrel.2015.10.049.

[8] M. Chen, G. Quan, Y. Sun, D. Yang, X. Pan, C. Wu, Nanoparticles-encapsulated polymeric microneedles for transdermal drug delivery, J. Control. Release 325 (2020) 163–175, https://doi.org/10.1016/j.jconrel.2020.06.039.

[9] Y.G. Anissimov, O.G. Jepps, Y. Dancik, M.S. Roberts, Mathematical and pharmacokinetic modelling of epidermal and dermal transport processes, Adv. Drug Deliv. Rev. 65 (2013) 169–190, https://doi.org/10.1016/j.addr.2012.04.009.

[10] W. Zhan, M. Alamer, X.Y. Xu, Computational modelling of drug delivery to solid tumour: understanding the interplay between chemotherapeutics and biological system for optimised delivery systems, Adv. Drug Deliv. Rev. 132 (2018) 81–103, https://doi.org/10.1016/j.addr.2018.07.013.

[11] M.S. Roberts, S.E. Cross, Y.G. Anissimov, Factors affecting the formation of a skin reservoir for topically applied solutes, Skin Pharmacol. Physiol. 17 (2004) 3–16, https://doi.org/10.1159/000074057.

[12] J.J. Calcutt, Y.G. Anissimov, Predicting viable skin concentration: diffusional and convective drug transport, J. Pharm. Sci. 110 (2021) 2823–2832, https://doi.org/10.1016/j.xphs.2021.03.012.

[13] K. Kretsos, G.B. Kasting, A geometrical model of dermal capillary clearance, Math. Biosci. 208 (2007) 430–453, https://doi.org/10.1016/j.mbs.2006.10.012.

[14] J.J. Calcutt, M.S. Roberts, Y.G. Anissimov, Predicting viable skin concentration: modelling the subpapillary plexus, Pharm. Res. 39 (2022) 783–793, https://doi.org/10.1007/s11095-022-03215-z.

[15] Y.G. Anissimov, M.S. Roberts, Modelling dermal drug distribution after topical application in human, Pharm. Res. 28 (2011) 2119–2129, https://doi.org/10.1007/s11095-011-0437-2.

[16] S.A. Machekposhti, M. Soltani, P. Najafizadeh, S.A. Ebrahimi, P. Chen, Biocompatible polymer microneedle for topical/dermal delivery of tranexamic acid, J. Control. Release 261 (2017) 87–92, https://doi.org/10.1016/j.jconrel.2017.06.016.

[17] B.R. Masters, P.T.C. So, Confocal microscopy and multi-photon excitation microscopy of human skin in vivo, Opt. Express 8 (2001) 2–10, https://doi.org/10.1364/oe.8.000002.

[18] X. Li, R. Johnson, B. Weinstein, E. Wilder, E. Smith, G.B. Kasting, Dynamics of water transport and swelling in human stratum corneum, Chem. Eng. Sci. 138 (2015) 164–172, https://doi.org/10.1016/j.ces.2015.08.009.

[19] W. Zhan, W. Gedroyc, X.Y. Xu, Effect of heterogeneous microvasculature distribution on drug delivery to solid tumour, J. Phys. D. Appl. Phys. 47 (2014), 475401, https://doi.org/10.1088/0022-3727/47/47/475401.

[20] M. Skobe, M. Detmar, Structure, function, and molecular control of the skin lymphatic system, J. Investig. Dermatol. Symp. Proc. 5 (2000) 14–19, https://doi.org/10.1046/j.1087-0024.2000.00001.x.

[21] L.T. Baxter, R.K. Jain, Transport of fluid and macromolecules in tumors. I. Role of interstitial pressure and convection, Microvasc. Res. 37 (1989) 77–104, https://doi.org/10.1016/0026-2862(89)90074-5.

[22] T. Waghule, G. Singhvi, S.K. Dubey, M.M. Pandey, G. Gupta, M. Singh, K. Dua, Microneedles: a smart approach and increasing potential for transdermal drug

[23] J.H. Jung, S.G. Jin, Microneedle for transdermal drug delivery: current trends and fabrication, J. Pharm. Investig. 51 (2021) 503–517, https://doi.org/10.1007/s40005-021-00512-4.

[24] M.C. Chen, Z.W. Lin, M.H. Ling, Near-infrared light-activatable microneedle system for treating superficial tumors by combination of chemotherapy and photothermal therapy, ACS Nano 10 (2016) 93–101, https://doi.org/10.1021/acsnano.5b05043.

[25] K. McLean, W. Zhan, Mathematical modelling of nanoparticle-mediated topical drug delivery to skin tissue, Int. J. Pharm. 611 (2022), 121322, https://doi.org/10.1016/j.ijpharm.2021.121322.

[26] Y.-M.F. Goh, H.L. Kong, C.-H. Wang, Simulation of the delivery of doxorubicin to hepatoma, Pharm. Res. 18 (2001) 761–770, https://doi.org/10.1023/A:1011076110317.

[27] C.S. Teo, W.H.K. Tan, T. Lee, C.H. Wang, Transient interstitial fluid flow in brain tumors: effect on drug delivery, Chem. Eng. Sci. 60 (2005) 4803–4821, https://doi.org/10.1016/j.ces.2005.04.008.

[28] K. Kretsos, G.B. Kasting, Dermal capillary clearance: physiology and modeling, Skin Pharmacol. Physiol. 18 (2005) 55–74, https://doi.org/10.1159/000083706.

[29] D.W. De Kort, J.P.M. Van Duynhoven, F.J.M. Hoeben, H.M. Janssen, H. Van As, NMR nanoparticle diffusometry in hydrogels: enhancing sensitivity and selectivity, Anal. Chem. 86 (2014) 9229–9235, https://doi.org/10.1021/ac502211q.

[30] T. Huang, S. Hsu, S. Chang, Molecular interaction mechanisms of glycol chitosan self-healing hydrogel as a drug delivery system for gemcitabine and doxorubicin, Comput. Struct, Biotechnol. J. 20 (2022) 700–709, https://doi.org/10.1016/j.csbj.2022.01.013.

[31] W. Zhan, C.-H. Wang, Convection enhanced delivery of liposome encapsulated doxorubicin for brain tumour therapy, J. Control. Release 285 (2018) 212–229, https://doi.org/10.1016/j.jconrel.2018.07.006.

[32] D.C. Wu, C.M. Ofner, Adsorption and degradation of doxorubicin from aqueous solution in polypropylene containers, AAPS PharmSciTech 14 (2013) 74–77, https://doi.org/10.1208/s12249-012-9885-1.

[33] P. Boderke, K. Schittkowski, M. Wolf, H.P. Merkle, Modeling of diffusion and concurrent metabolism in cutaneous tissue, J. Theor. Biol. 204 (2000) 393–407, https://doi.org/10.1006/jtbi.2000.2023.

[34] W. Zhan, X.Y. Xu, A mathematical model for thermosensitive liposomal delivery of doxorubicin to solid tumour, J. Drug Deliv. 2013 (2013), https://doi.org/10.1155/2013/172529.

[35] S. Eikenberry, A tumor cord model for doxorubicin delivery and dose optimization in solid tumors, Theor. Biol. Med. Model. 6 (2009) 16, https://doi.org/10.1186/1742-4682-6-16.

[36] V.P. Chauhan, T. Stylianopoulos, J.D. Martin, Z. Popović, O. Chen, W.S. Kamoun, M.G. Bawendi, D. Fukumura, R.K. Jain, Normalization of tumour blood vessels improves the delivery of nanomedicines in a size-dependent manner, Nat. Nanotechnol. 7 (2012) 383–388, https://doi.org/10.1038/nnano.2012.45.

[37] W. Zhang, J. Gao, Q. Zhu, M. Zhang, X. Ding, X. Wang, X. Hou, W. Fan, B. Ding, X. Wu, X. Wang, S. Gao, Penetration and distribution of PLGA nanoparticles in the human skin treated with microneedles, Int. J. Pharm. 402 (2010) 205–212, https://doi.org/10.1016/j.ijpharm.2010.09.037.

[38] T.W.H. Sheu, M.A. Solovchuk, A.W.J. Chen, M. Thiriet, On an acoustics–thermal–fluid coupling model for the prediction of temperature elevation in liver tumor, Int. J. Heat Mass Transf. 54 (2011) 4117–4126, https://doi.org/10.1016/j.ijheatmasstransfer.2011.03.045.

[39] W.P. Paaske, Absence of restricted diffusion in adipose tissue capillaries, Acta Physiol. Scand. 100 (1977) 430–436, https://doi.org/10.1111/j.1748-1716.1977.tb05967.x.

[40] E.A. Swabb, J. Wei, P.M. Gullino, Diffusion and convection in normal and neoplastic tissues, Cancer Res. 34 (1974) 2814–2822.

[41] J. Chen, F. Zehtabi, J. Ouyang, J. Kong, W. Zhong, M.M.Q. Xing, Reducible self-assembled micelles for enhanced intracellular delivery of doxorubicin, J. Mater. Chem. 22 (2012) 7121–7129, https://doi.org/10.1039/C2JM15277K.

[42] N. Seko, H. Bando, C.W. Lim, F. Yamashita, M. Hashida, Theoretical analysis of the effect of cutaneous metabolism on skin permeation of parabens based on a two-layer skin diffusion/metabolism model, Biol. Pharm. Bull. 22 (1999) 281–287, https://doi.org/10.1248/bpb.22.281.

[43] L.D. Mayer, L.C.L. Tai, D.S.C. Ko, D. Masin, R.S. Ginsberg, P.R. Cullis, M.B. Bally, Influence of vesicle size, lipid composition, and drug-to-lipid ratio on the biological activity of liposomal doxorubicin in mice, Cancer Res. 49 (1989) 5922–5930.

[44] T.M. Allen, T. Mehra, C. Hansen, Y.C. Chin, Stealth liposomes: an improved sustained release system for 1-β-d-arabinofuranosylcytosine, Cancer Res. 52 (1992) 2431–2439.

[45] T. Tagami, M.J. Ernsting, S. Li, Optimization of a novel and improved thermosensitive liposome formulated with DPPC and a Brij surfactant using a robust in vitro system, J. Control. Release 154 (2011) 290–297, https://doi.org/10.1016/j.jconrel.2011.05.020.

[46] J. Connor, M.B. Yatvin, L. Huang, pH-sensitive liposomes: acid-induced liposome fusion, Proc. Natl. Acad. Sci. 81 (1984) 1715–1718, https://doi.org/10.1073/pnas.81.6.1715.

[47] E. Garcion, A. Lamprecht, B. Heurtault, A. Paillard, A. Aubert-Pouessel, B. Denizot, P. Menei, J.-P. Benoît, A new generation of anticancer, drug-loaded, colloidal vectors reverses multidrug resistance in glioma and reduces tumor progression in rats, Mol. Cancer Ther. 5 (2006) 1710–1722, https://doi.org/10.1158/1535-7163.MCT-06-0289.

[48] T. Tagami, J.P. May, M.J. Ernsting, S.-D. Li, A thermosensitive liposome prepared with a Cu2+ gradient demonstrates improved pharmacokinetics, drug delivery and

antitumor efficacy, J. Control. Release 161 (2012) 142–149, https://doi.org/10.1016/j.jconrel.2012.03.023.

[49] M. Kumar, D. Gupta, G. Singh, S. Sharma, M. Bhat, C.K. Prashant, A.K. Dinda, S. Kharbanda, D. Kufe, H. Singh, Novel polymeric nanoparticles for intracellular delivery of peptide cargos: antitumor efficacy of the BCL-2 conversion peptide NuBCP-9 delivery of NuBCP in polymeric nanoparticles, Cancer Res. 74 (2014) 3271–3281, https://doi.org/10.1158/0008-5472.CAN-13-2015.

[50] L.X. Xu, A. Zhang, X. Mi, Study of thermally targeted nano-particle drug delivery for tumor therapy, Int. Conf. Micro/Nanoscale Heat Transf. 42924 (2008) 1399–1406, https://doi.org/10.1115/MNHT2008-52383.

[51] A. Ziemys, S. Klemm, M. Milosevic, K. Yokoi, M. Ferrari, A. Ziemys, S. Klemm, M. Milosevic, K. Yokoi, M. Ferrari, M. Kojic, Computational analysis of drug transport in tumor microenvironment as a critical compartment for nanotherapeutic pharmacokinetics, Drug Deliv. 23 (2016) 2524–2531, https://doi.org/10.3109/10717544.2015.1022837.

[52] C. Wong, T. Stylianopoulos, J. Cui, J. Martin, V.P. Chauhan, W. Jiang, Z. Popovic, Multistage nanoparticle delivery system for deep penetration into tumor tissue, Proc. Natl. Acad. Sci. 108 (2011) 2426–2431, https://doi.org/10.1073/pnas.1018382108.

[53] T. Wagner, A. Kroll, C.R. Haramagatti, H.-G. Lipinski, M. Wiemann, Classification and segmentation of nanoparticle diffusion trajectories in cellular micro environments, PLoS One 12 (2017), e0170165, https://doi.org/10.1371/journal.pone.0170165.

[54] E. Parrish, M.A. Caporizzo, R.J. Composto, Network confinement and heterogeneity slows nanoparticle diffusion in polymer gels, J. Chem. Phys. 146 (2017), 203318, https://doi.org/10.1063/1.4978054.

[55] C.W. Gan, S. Feng, Biomaterials polyethylene glycol succinate diblock copolymer for targeted drug delivery across the blood e brain barrier, Biomaterials. 31 (2010) 7748–7757, https://doi.org/10.1016/j.biomaterials.2010.06.053.

[56] K.Y. Win, S. Feng, Effects of particle size and surface coating on cellular uptake of polymeric nanoparticles for oral delivery of anticancer drugs, Biomaterials. 26 (2005) 2713–2722, https://doi.org/10.1016/j.biomaterials.2004.07.050.

[57] M.M. Schmidt, K.D. Wittrup, A modeling analysis of the effects of molecular size and binding affinity on tumor targeting, Mol. Cancer Ther. 8 (2009) 2861–2871, https://doi.org/10.1158/1535-7163.MCT-09-0195.

[58] F. Yurt, M. Ince, S.G. Colak, K. Ocakoglu, O. Er, H.M. Soylu, C. Gunduz, C.B. Avci, C.C. Kurt, Investigation of in vitro PDT activities of zinc phthalocyanine immobilised TiO2 nanoparticles, Int. J. Pharm. 524 (2017) 467–474, https://doi.org/10.1016/j.ijpharm.2017.03.050.

[59] Q.Y. Bao, A.Y. Liu, Y. Ma, H. Chen, J. Hong, W. Bin Shen, C. Zhang, Y. Ding, The effect of oil-water partition coefficient on the distribution and cellular uptake of liposome-encapsulated gold nanoparticles, Colloids Surf. B: Biointerfaces 146 (2016) 475–481, https://doi.org/10.1016/j.colsurfb.2016.06.046.

[60] A. Singh, S. Yadav, Microneedling : advances and widening horizons, Indian Dermatol. Online J. 7 (2016) 244–254, https://doi.org/10.4103/2229-5178.185468.

[61] R. Mishra, T.K. Maiti, T.K. Bhattacharyya, Development of SU-8 hollow microneedles on a silicon substrate with microfluidic interconnects for transdermal drug delivery, J. Micromech. Microeng. 28 (2018), 105017, https://doi.org/10.1088/1361-6439/aad301.

[62] M.Y. Chen, Y.Y. Chen, H.T. Tsai, T.S. Tzai, M.C. Chen, Y.S. Tsai, Transdermal delivery of luteinizing hormone-releasing hormone with chitosan microneedles: a promising tool for androgen deprivation therapy, Anticancer Res. 37 (2017) 6791–6797, https://doi.org/10.21873/anticanres.12139.

[63] A. Kamath, A. Laha, S. Pandiyan, S. Aswath, A. Kishore, P. Dey, Atomistic investigations of polymer-doxorubicin-CNT compatibility for targeted cancer treatment : a molecular dynamics study, J. Mol. Liq. 348 (2022), 118005, https://doi.org/10.1016/j.molliq.2021.118005.

[64] S.W. Chung, G.C. Kim, S. Kweon, H. Lee, J.U. Choi, F. Mahmud, H.W. Chang, J.W. Kim, W.C. Son, S.Y. Kim, Y. Byun, Metronomic oral doxorubicin in combination of Chk1 inhibitor MK-8776 for p53-deficient breast cancer treatment, Biomaterials. 182 (2018) 35–43, https://doi.org/10.1016/j.biomaterials.2018.08.007.

[65] X. Zhang, X. Sun, J. Li, X. Zhang, T. Gong, Z. Zhang, Lipid nanoemulsions loaded with doxorubicin-oleic acid ionic complex: characterization, in vitro and in vivo studies, Die Pharm. Int. J. Pharm. Sci. 66 (2011) 496–505, https://doi.org/10.1691/ph.2011.0379.

[66] D. Missirlis, R. Kawamura, N. Tirelli, J.A. Hubbell, Doxorubicin encapsulation and diffusional release from stable, polymeric, hydrogel nanoparticles, Eur. J. Pharm. Sci. 29 (2006) 120–129, https://doi.org/10.1016/j.ejps.2006.06.003.

[67] D. Wheeler, C. Wilkinson, From calm to storm: the origins of the Beaufort wind scale, Mar. Mirror. 90 (2004) 187–201, https://doi.org/10.1080/00253359.2004.10656896.

[68] C. Lei, P. Davoodi, W. Zhan, P.K.-H. Chow, C.-H. Wang, Development of nanoparticles for drug delivery to brain tumor: the effect of surface materials on penetration into brain tissue, J. Pharm. Sci. 108 (2019) 1736–1745, https://doi.org/10.1016/j.xphs.2018.12.002.

[69] W. Zhan, D.Y. Arifin, T.K. Lee, C.H. Wang, Mathematical modelling of convection enhanced delivery of carmustine and paclitaxel for brain tumour therapy, Pharm. Res. 34 (2017) 860–873, https://doi.org/10.1007/s11095-017-2114-6.

[70] S.H. Ranganath, Y. Fu, D.Y. Arifin, I. Kee, L. Zheng, H.S. Lee, P.K.H. Chow, C.H. Wang, The use of submicron/nanoscale PLGA implants to deliver paclitaxel with enhanced pharmacokinetics and therapeutic efficacy in intracranial glioblastoma in mice, Biomaterials. 31 (2010) 5199–5207, https://doi.org/10.1016/j.biomaterials.2010.03.002.

[71] A. Bhandari, A. Bansal, A. Singh, N. Sinha, Perfusion kinetics in human brain tumor with DCE-MRI derived model and CFD analysis, J. Biomech. 59 (2017) 80–89, https://doi.org/10.1016/j.jbiomech.2017.05.017.

[72] K.B. Neeves, C.T. Lo, C.P. Foley, W.M. Saltzman, W.L. Olbricht, Fabrication and characterization of microfluidic probes for convection enhanced drug delivery, J. Control. Release 111 (2006) 252–262, https://doi.org/10.1016/j.jconrel.2005.11.018.

[73] K. Parsi, H. Partsch, E. Rabe, A.A. Ramelet, Reticulate eruptions. Part 1: vascular networks and physiology, Australas. J. Dermatol. 52 (2011) 159–166, https://doi.org/10.1111/j.1440-0960.2011.00749.x.

[74] H.S. Min, Y. Kim, J. Nam, H. Ahn, M. Kim, G. Kang, M. Jang, H. Yang, H. Jung, Shape of dissolving microneedles determines skin penetration ability and efficacy of drug delivery, Biomater. Adv. 145 (2023), 213248, https://doi.org/10.1016/j.bioadv.2022.213248.

[75] P. Makvandi, M. Kirkby, A.R.J. Hutton, M. Shabani, C.K.Y. Yiu, Z. Baghbantaraghdari, R. Jamaledin, M. Carlotti, B. Mazzolai, V. Mattoli, Engineering microneedle patches for improved penetration: analysis, skin models and factors affecting needle insertion, Nano-Micro Lett. 13 (2021) 93, https://doi.org/10.1007/s40820-021-00611-9.